Title

MOLECULAR BEAM KINETICS. I. MAGNETIC DEFLECTION ANALYSIS OF REACTIONS OF li WITH Cl2, IC1, Br2, SnCl4, AND PCl3

Authors

Parrish, David D.
Henn, Ronald R.

Publication Date

1969-06-01

Submitted to J. of Chemical Physics

UCRL-19036
Preprint

cy. 2

MOLECULAR BEAM KINETICS. I. MAGNETIC DEFLECTION ANALYSIS OF REACTIONS OF Li WITH Cl_2, ICl, Br_2, $SnCl_4$, AND PCl_3

David D. Parrish and Ronald R. Herm

June 1969

AEC Contract No. W-7405-eng-48

LAWRENCE RADIATION LABORATORY
UNIVERSITY of CALIFORNIA BERKELEY

UCRL-19036

cy. 2

DISCLAIMER

MOLECULAR BEAM KINETICS. I. MAGNETIC DEFLECTION ANALYSIS OF REACTIONS OF Li WITH Cl_2, ICl, Br_2, $SnCl_4$, and PCl_3

David D. Parrish and Ronald R. Herm

Inorganic Materials Research Division
of the Lawrence Radiation Laboratory
and
Department of Chemistry, University of
California, Berkeley, California

ABSTRACT

Thermal energy crossed molecular beam studies have been made of the reactions of Li with Cl_2, ICl, Br_2, $SnCl_4$, and PCl_3. An inhomogeneous deflecting magnet between the collision zone and detector was used to distinguish elastic scattering of Li from reactive scattering of LiX. Approximate transformations of the measured laboratory angular distributions to the center-of-mass (CM) coordinate system have determined: (1) the total reaction cross sections, Q_R; (2) the approximate product recoil energies, E'; (3) the reactive attenuations of the wide-angle

elastic scattering; and (4) the LiX product CM angular distributions. A procedure has been developed for the determination of values of Q_R which corrects for resolution effects introduced by broad parent alkali beam profiles. Values of Q_r, E', and reactive attenuations of wide-angle elastic scattering which are reported here for the Li atom reactions correlate roughly with trends established in previous studies of the reactions of Na, K, Rb, and Cs. However, the observed LiX CM product angular distributions are broader and more complex than projections based on studies with the heavier alkali atoms might have predicted. These observations are interpreted in terms of the electron transfer mechanism, which has been applied in previous studies of reactions of the heavier alkali atoms, with the inclusion of a possible mass effect in the alkali atom reaction dynamics.

Extensive data on the reactions of K, Rb, and Cs with halogen containing compounds have been provided in the past few years by molecular beam techniques.[1] A wealth of data was provided on the reaction kinetics of Na atoms by the early Polanyi diffusion flame studies[2], and a recent crossed beam study of Na atom reactions has been reported[3]. Molecular beam studies have determined total and differential cross sections for the elastic scattering of Li atoms[4], including total cross section determinations with highly reactive halogen containing compounds as the collision partners[5]; however, no previous crossed beam studies of the reactive scattering of Li compounds have been reported[6,7]. Indeed, it would appear that no previous studies of gas phase Li atom reaction kinetics have been reported, although Ljalikov and Tererin[8,9] did report the observation of chemilumescence from a gas phase mixture of Li and I_2. This paper describes results obtained from angular distribution measurements for the reactions of Li with Cl_2, ICl, Br_2, $SnCl_4$, and PCl_3. Although very detailed beam studies have been reported for the reactions of heavier alkali atoms with some of these compounds, the results reported here for Li reactions

will be compared with the more primitive beam results on Na, K, Rb, and Cs reactions[10] in order to provide comparisions of the reaction features for the five alkali metals obtained under similar experimental conditions.

It is anticipated that the study reported here will be the precursor of more detailed beam comparisons of the reactions of Li and Na atoms. Previous alkali atom reaction studies have been interpreted[1, 11] in terms of an electron transfer mechanism due originally to M. Polanyi and Magee; in this model, the dominant long range forces between the reactants are determined by the ionization potential of the alkali atom and the vertical electron affinity of the reacting gas. Since this mechanism also accounts qualitatively for the features of the Li atom reactions observed in this study and since the ionization potentials are quite similar for Na and Li, a comparison of the features of the reactions of these two atoms might reflect the role of mass effects in the overall reaction dynamics.

EXPERIMENTAL CONDITIONS

The apparatus and experimental procedures used were similar to those employed in previous magnetic deflection analysis studies of the reactions of the heavier alkali metals.[12] The apparatus shown in Fig. 1 was enclosed in a copper box attached to a large liquid nitrogen reservoir[13]. The reactant gas was prepared on an external line at the desired pressure (typically ~3 Torr) and emerged from a variable temperature, "crinkly

foil" many-channel source (~0.012 cm hole radius, ~0.5 cm long, calculated porosity ~ 90%) with a roughly triangular 13° FWHM beam profile; the collimating slits required warning somewhat to prevent clogging. The Li source was a conventional stainless steel two-chamber oven equipped with standard knife-edged slits.

Studies[10] of the reactive scattering of Na, K, Rb, and Cs have employed two-filament differential surface ionization to measure the scattered M and MX signals separately; a previous surface ionization study[14] had indicated that differential surface ionization might also be used to distinguish Li from LiI. However, the differential surface ionization detection technique proved impractical in this study due to the extremely poor ionization efficiency of Li atoms on a "methanated" Pt-8% W surface. Instead, the magnetic deflection technique was used to distinguish Li and LiX, both of which were surface ionized on a continuously oxygenated W filament. Data presented later, as well as results of Ref. 14, indicate that this surface ionizes Li and LiX with comparable efficiencies. In partial agreement with previous work[15], we found that this surface achieved its maximum ionization efficiency and best signal to noise ratio when operated at a fairly low temperature (~ 1700° K), possibly due to the formation of a stable oxide layer on the surface.

When energized, the inhomogeneous electromagnet[16] placed between the collision zone and detector deflected aside a known fraction of the Li atoms, thereby providing a measure of the

scattered Li and LiX separately. The entire magnet assembly was shielded in such a way that only Li or LiX scattered out of the collision volume defined by the two intersecting beams could reach the detector. As discussed in Ref. 12, this shielding of the detector assembly had the added benefit of protecting the surface ionization filament from any detectable "poisoning" effects. Checks of the beam profile for the parent Li beam and scattered signals at various laboratory (LAB) angles were taken periodically; except at angles near the parent gas beam, these profiles were found to conform to that predicted by the magnet collimating slit geometry, except for a negligible broadening of the wings of the profile produced by collisions with the ambient background gas after passage through the first collimating slit (due to the continuous oxygenation of the W filament, the apparatus pressure was typically $\sim 1.5\ 10^{-6}$ Torr). For LAB angles within the profile of the gas beam, a higher background pressure was produced within the deflecting magnet collimating slit assembly. This produced a pressure broadening of the undeflected beam profile of the scattered signals for this range of Θ, thereby producing an angle dependent transmission function[17] (the transmission T_H is defined as the ratio of Li signal with the magnet energized to the undeflected Li beam intensity, measured at the center of the undeflected beam profile).

As illustrated in Fig. 1, the Li^+ produced by surface ionization of Li or LiX was mass analyzed in a 2.54 cm. radius electromagnet[18,19]. Experiments were run in a low resolution mode of this spectrometer; Li^6 and Li^7 were not resolved, but

the Li^+ signal was clearly resolved from the other alkali ions in the background noise spectrum. Since a high concentration of Li_2 in the Li beam would have proved troublesome in interpreting these experiments, the upper Li oven chamber was held at a considerably higher temperature than the lower chamber. Typically, these chambers were held at 950°K and 1075°K; at thermal equilibrium, this would correspond to a Li source pressure of ~0.3 Torr, with less than 0.5% Li_2 in the effusing beam. Magnetic deflection typically attenuated the parent Li beam by 99%, indicating a neglible concentration of Li_2 in the beam provided that it was surface ionized to give Li^+ rather than Li_2^+. An auxiliary experiment, employing velocity and magnetic deflection analysis of the parent Li beam, confirmed that indeed Li_2 did give a surface ionization signal of Li^+ and thus that the Li_2 concentration in these experiments was negligible.

The experimental procedure, described in Ref. 12, consisted in measurements of the scattered intensity as a function of LAB angle at zero deflecting magnetic field and at a standard high deflecting magnetic field, H (about 15 kG with a gradient of about 90 kG/cm). These two scattered signals were converted to relative intensities, $I_0^M(\Theta)$ and $I_H^M(\Theta)$, by dividing them by the absolute attenuation of the Li beam produced by the crossed beam; experiments were always run at a relative Li beam attenuation of less than 10%. The Li and LiX angular distributions were calculated in turn from the experimentally measured quantities as follows:

$$I^M_{Li} = \frac{I^M_O - I^M_H}{1 - T_H} \qquad (1a)$$

$$I^M_{LiX} = \frac{I^M_H - T_H\, I^M_O}{1 - T_H} . \qquad (1b)$$

The transmission of Li atoms through the magnet, $T_H(\Theta)$, was determined periodically by measuring the transmission versus Θ of a Li atom beam which had been scattered from the non-reactive gas cyclohexane.

The angular distributions calculated according to Eqs. (1) were distorted by a viewing factor correction which arose because the detector saw only a Θ dependent fraction of the total scattering volume through the collimating slits of the deflecting magnet. The true Li and LiX angular distributions were calculated from the distributions determined from Eqs. (1) by multiplying by a viewing factor correction defined as

$$V(\Theta) = \frac{\text{total scattering volume}}{\text{effective scattering volume seen by the detector}} . \qquad (2)$$

Theoretical values of $V(\Theta)$ calculated from slit geometries and from experimentally determined beam profiles are indicated in Fig. 2; these calculated values of V are almost symmetric about $\Theta = 0°$ and $\Theta = 90°$. These data indicate the importance of this correction, since V varies over a factor of 5 to 10 as Θ goes

from 0° to 90°. However, these theoretical values of V (Θ) were not used to correct I^M_{Li} (Θ) and I^M_{LiX} (Θ). Rather, values of V (Θ) were determined individually for each reactive scattering experiment by measuring the relative intensity of scattered signal from the same scattering gas, I (Θ), with the deflecting magnet and its collimating slits removed; in this case,

$$V(\Theta) = I(\Theta)/I^M_0(\Theta).$$

Figure 2 indicates that the average of these measured values of V (Θ) does agree roughly with the theoretical values. The lack of symmetry about Θ = 90° as well as the large standard deviations in the measured V (Θ) curve are thought to arise from small, random, and inconsequential misalignments of the deflecting magnet collimating slits with respect to the center of rotation of the oven assembly (COR). The departure of the experimental and calculated V (Θ) curves at small LAB angles is thought to be a resolution effect which arises because removal of the magnet slits reduces the effective angular resolution of the parent Li beam considerably, and thus alters the form of the small angle elastic scattering intensity.

As a check of the techniques employed in this study against the more convential two-filament differential surface ionization studies, the angular distribution of NaBr formed in the scattering of Na from Br_2 was measured. Comparison with the data of Ref. 3 is shown in Fig. 3; the overall shape of the curve as well as the peak position is well reproduced. This calibration

experiment was run before centain modifications were incorporated to improve the signal to noise ratio in the apparatus; for this reason, the data in Fig. 3 is noisier and restricted to a narrower range of Θ values than is the data reported for the Li reactions.

Figure 4 shows the primary data for Li + Br_2, collected during three different experiments, at different absolute signal levels. The agreement at narrow angles between results of different experiments, the agreement between calculated and experimental viewing factors shown in Fig. 2, the calibration data shown in Fig. 3, and comparisons of the experimental and theoretical narrow angle elastic scattering angular distributions to be shown in a later section all indicate an absence of any appreciable non-linear detector response. The scatter in the wide angle non-reactive scattering data shown in Fig. 4 illustrates one of the handicaps of the magnetic deflection analysis technique. In the study of scattering partners with large reactive cross sections, the wide angle elastic scattering is severely attenuated; consequently, $I_O^M(\Theta)$ and $I_H^M(\Theta)$ differ only slightly. In this case, Eq. (1a) illustrates that relatively small errors in individual determinations of $I_O^M(\Theta)$ and $I_H^M(\Theta)$ can result in a very large uncertainty in the derived non-reactive scattering intensity. For this reason, the derived non-reactive scattering distribution shown in Fig. 4 is of limited quantitative use, but does indicate that the predominate scattered species at wide laboratory angles in LiBr rather than Li. Figure 5 gives similar primary data for the other reactions studied.

RESULTS AND KINEMATIC ANALYSIS

Elastic Scattering

Figure 6 shows the CM elastic scattering of Li atoms obtained by transforming the LAB angular distributions by the conventional procedure[10a] of assigning to the two scattering partners their most probable source velocities and assuming that all non-reactive scattering was due to elastic collisions. As indicated in Fig. 6, the two CM branches do give the same intensity, except at points obtained by transforming wide negative LAB angles where the approximate transformation procedure employed is known to be especially bad.[10a] These curves illustrate that the wide-angle elastic scattering of Li from Cl_2, ICl, Br_2, $SnCl_4$, and PCl_3 falls off much more rapidly than does the elastic scattering produced by the non-reactive gas cyclohexane; this reactive attenuation of the wide-angle elastic scattering was previously observed in studies of the reactions of the heavier alkali metals.[1] Figure 6 also illustrates that the wide angle falloff is similar for all five reactive gases studied here. In view of the large uncertainty in the wide angle LAB data shown in Figs. 4 and 5, further quantitative comparisons of the data shown in Fig. 6 could be misleading.

Reactive Scattering

Figures 7 - 11 show the LAB angular distributions of the lithium halide products. Also shown are kinematic diagrams indicating LiX recoil velocities for a few of the possible final relative translational product recoil energies, E'. The total energy available to the products must be partitioned between E' and internal excitation W' and is given by

$$E' + W' = E + W + \Delta D_o,$$

where E + W is the initial thermal reactant energy and ΔD_o is the difference in LiX and R-X bond dissociation energies. The error bars on each figure[20] indicate the difficulty of obtaining reliable product angular distributions in the small angle range ($|\Theta| \lesssim 10°$). In this range, the elastic scattering is typically ten to a hundred times more intense than is the reactive scattering; as Eq. (1b) illustrates, a small error in the auxilliary determination of the transmission of Li atoms through the magnet can result in a large uncertainty in the derived product angular distribution under these conditions. Nevertheless, the magnetic deflection analysis techniques seems to do at least as well in this angular range as does the more conventional differential surface ionization technique (compare with product distributions reported in Ref. 10); it has the added advantage that it is an absolute measurement and does not rely on the variation of a normalization parameter, as has sometimes been necessary in differential surface ionization

studies[3,10] to obtain a smooth product distribution near $\Theta = 0°$. However, for two experiments, the narrow angle scattering was also analyzed with a slightly modified $T_H(\Theta)$ function (the solid symbols of Figs. 8 and 10). Evidently, $T_H(\Theta)$ changed slightly between the calibration and reactive runs during these experiments.

In studies with the heavier alkali metals, these five reactants have provided prototype examples of "stripping" reactions[1a], with the product angular distributions sharply peaked in the original alkali atom direction ($\theta = 0°$). Figures 7-11 show the distributions in centroid angles, resulting from the thermal velocity distributions in both beams[21], calculated for an energy independent collision cross section according to the method of Ref. 22. As these figures indicate, the diatomic reactants yield LAB product distribution confined mainly to the left of the centroid distributions; this must indicate a predominant scattering into the forward hemisphere ($0° \leq \theta \leq 90°$) in the CM coordinate system, in qualitative agreement with the results found for the heavier alkali atoms. In contrast, the polyatomic reactants yield appreciable LAB product intensity to the right of the centroid distribution, indicative of appreciable product scattering into the backward hemisphere in the CM system. The dip in the LAB distribution for Li + Br_2 near $\Theta = 0°$ is thought to be real, although it occurs in the angular range where uncertainties introduced by measurements of the transmission factor are highest[23]. However, the relatively flat portions of the LAB distributions for Li + $SnCl_4$ and PCl_3

which extend through $\Theta = 0°$ are definitely present because these flat portions extend into ranges of Θ where the data is not particularly sensitive to small errors in $T_H(\Theta)$ and is thought to be best.

The LAB product angular distributions were transformed to the CM (Figs. 12 and 13) by the same fixed velocity approximation (FVA) procedure used to transform the elastic scattering. Here again the reactants were assumed to have their most probable source velocities, and the final recoil energy E' was varied as a parameter until a consistent CM angular distribution was obtained. Extensive computer studies[24] have indicated that the CM angular distributions obtained from the FVA procedure are usually reliable, although somewhat broader than the true distributions; the values of E' derived may be relatively inaccurate (somewhat too low), although they do usually suffice to indicate the qualitative features of the energy partitioning.

Table I lists values of product recoil energies derived by the FVA transformation procedure and compares these results with values of E' reported for Na, K, Rb, and Cs reactions in Ref. 10; no values of E' were reported for Rb + PCl_3 or Cs + $SnCl_4$, although it was reported that the MX recoil energies were ~ 10% to ~ 30% of the reaction exothermicities[10e]. Note that these experiments cannot distinguish MCl and MI products of the M + ICl reaction; crossed beam chemiluminescence experiments indicate that KCl is the principal product of the K + ICl reaction.[25] These values of E' illustrate that, for all of these reactions, most of the reaction exothermicity

appears as internal excitation in the products. Moreover, for Cl_2 and Br_2, the data does indicate a trend to higher product recoil energies as the mass of the attacking alkali atom decreases.

Table II gives the coefficients of an expansion of the LiX CM angular distributions shown in Figs. 12 and 13 in terms of the Legendre polynomials. As a partial check of these derived CM LiX distributions, they were used to back-calculate the LAB distributions by holding E' fixed at the values given in Table I and averaging over the velocity distributions in both beams. The extent of agreement between these back-calculated distributions and the measured distributions are shown in Figs. 7 - 11. Variations of E' during these back-calculations indicated that the FVA derived E' values given in Table I do give the best delta function approximations to the true E' distributions produced by these reactions.

Previous studies[10] with Na, K, Rb, and Cs have indicated an almost monotonous forward peaking of the MX product for these five reactants, although the polyhalide reactants did produce a less sharp MX peaking at $\theta = 0°$ and appreciably more product intensity at $\theta > 90°$ than did the diatomic reactants. For K, Rb, and Cs + Br_2 and Cl_2, the results suggested that the alkali atoms were so reactive as to have lost their chemical identity in the sense that the product angular distributions, while differing for Cl_2 and Br_2, were the same for K, Rb, and Cs (although this was not the case for K, Rb and Cs + ICl; see Ref. 10b). Figure 12 indicates that this is clearly not the

case for Li, as the LiX product distributions are very much broader than those produced by reactions of the heavier alkali atoms. Indeed, the Li + Cl_2, ICl, and Br_2 reactions have almost achieved the opposite extreme where the Li atom dominates the reaction features in the sense that, as indicated by the Legendre coefficients of Table II, the LiX angular distributions are almost superimposable for these three reactions.

For the polyhalide reactants, the Li atom results shown in Fig. 13 are in even more striking contrast with the behavior of the heavier alkali atoms. The LiCl CM distributions are severely broadened and no longer peak in the direction of the incident Li reactant. In fact, for Li + PCl_3, Fig. 11 indicates that the LAB data can be closely fit by a CM LiCl distribution which is symmetric about $\theta = 90°$; this is the behavior which would be exhibited by a reaction which had lost all of its direct interaction character and proceeded via formation of a long-lived intermediate complex.

Total Reaction Cross Sections

The total reactive cross section Q_R could be easily calculated if it were possible to measure the absolute density and scattering length of the crossed gas beam. However, since this determination was not possible here nor in previous studies with the heavier alkali atoms, indirect methods must be employed to determine Q_R; three methods which might be applicable to the present work were developed in Ref. 10c. In all three methods, Q_R is given by the integration of the CM differential reactive cross section

$$Q_R = 2\pi \int_0^{\pi} \left(\frac{\partial Q_R}{\partial \omega}\right)_{abs} \sin\theta \, d\theta. \qquad (3)$$

The absolute normalization of the differential cross section,

$$\left(\frac{\partial Q_R}{\partial \omega}\right)_{abs} = \kappa \; I_{LiX} \; (\theta), \qquad (4)$$

is determined by comparison of the measured elastic scattering signal with theoretical expressions for the cross section for elastic scattering from a van der Waals potential, $V(r) = -C/r^6$. However, only Methods A and B of Ref. 10c are applicable here; their Method C relies on measurements of the fraction of alkali atoms scattered out of the parent alkali beam. Due to the low ionization efficiency of Li relative to K, Rb, or Cs, it was felt that a measurement of this nature might be distorted by a non-linear detector response at the extremely high Li intensities encountered in the parent Li beam itself (these signal levels are 100 to 1000 more intense than are the narrow angle elastic scattering signals).

Method A

In Method A of Ref. 10c the normalization factor is evaluated by a comparison of the experimental and theoretical differential elastic cross sections,

$$\kappa = (\partial Q_e/\partial\omega)_{abs} \Big/ I_{Li}(\theta). \qquad (5)$$

The comparison is made at narrow angles where the elastic scattering is assumed to be negligibly perturbed by reaction and the small angle scattering formula for a van der Waals interaction is used,

$$(\partial Q_e/\partial\omega)_{abs} = 0.239\,(C/E)^{1/3}\,\theta^{-7/3}. \qquad (6)$$

However, the very broad and high Li beam employed in these experiments make it necessary to modify this procedure because the fall-off of small angle elastic scattering is no longer described by Eq. (6).

The procedure we have adopted[26], similar to Method A of Ref. 10c, proceeds by writing down the expressions for the relative intensities of Li and LiX species measured with a detector subtending a solid angle $\delta\Omega$ in the LAB system; since $(\partial Q_R / \partial\omega)_{abs}$ is only slowly varying with angle, the expression for $I_{LiX}(\theta)$ is given by

$$I_{LiX}(\theta) = \frac{4\beta F\, n\, h_o\, \xi_o\, \delta\ell\, \delta\Omega}{A} (\partial Q_R / \partial\omega)_{abs}. \qquad (7)$$

In this expression, it is assumed that the Li beam profile is rectangular, with a width of $2\,\xi_o$ and a height of $2\,h_o$ at the collision zone; $\delta\ell$ is the width of the crossed gas beam whose number density at the collision zone is n; F represents the

flux of incident Li atoms, A gives the absolute attenuation of the Li beam, and β represents the LiX surface ionization efficiency.

It is more convenient to express the relative signal for small angle elastic scattering in the LAB system; at very small angles ($\sin\theta = \theta$) and for a target gas at rest, the LAB to CM transformation for elastic scattering is given in terms of m/μ, the ratio of the mass of Li to the reduced mass of the collision partners, by:

$$\theta = (m/\mu)\ \Theta \tag{8a}$$

$$(\partial\omega/\partial\Omega) = m^2/\mu^2. \tag{8b}$$

Using these transformation equations and substituting $\langle E^{-1/3} \rangle$, the Boltzman average[10c] of $E^{-1/3}$, into Eq. (6), the differential cross section for scattering of a Li beam of infinitesimal width in the LAB becomes

$$\left(\frac{\partial Q_e}{\partial\Omega}\right)_{abs} = 0.216 \left(\frac{C}{kT_{Li}}\right)^{1/3} \Theta^{-7/3}. \tag{9}$$

An elastic scattering event in which the Li atom arrives at the detector ξ' to the side and h' above a line perpendicular to an idealized point source oven slit would be recorded as scattering through a small LAB angle

$$\Theta^2 = (h'^2 + \xi'^2) / \ell_2^2 \qquad (10)$$

where ℓ_2 is the distance from the collision zone to the detector. Had it not been deflected, this Li atom would have arrived at the detector at the point $(\gamma \xi_c, \gamma h_c)$ where $(\xi_c^2 + h_c^2)^{1/2}$ gives its radial deviation from perfect collimation at the collision zone and where

$$\gamma = (\ell_1 + \ell_2) / \ell_1 \qquad (11)$$

with ℓ_1 equal to the distance from the oven slit to the collision zone. Thus, the true scattering angle is given by

$$\Theta_t^2 = \ell_2^{-2} \left((h' - \gamma h_c)^2 + (\xi' - \gamma \xi_c)^2 \right). \qquad (12)$$

Since only in-plane scattering was measured here and the height and width of the detector were small relative to γh_o and $\gamma \xi_o$ respectively, h' may be put equal to zero and the scattered flux may be considered uniform over $\delta\Omega$. Recognizing this, the total relative signal scattered into the detector for small Θ may be written as

$$I_{Li}(\Theta) = 2B \int_{-\xi_o}^{\xi_o} d\xi_c \int_0^{h_o} \frac{dh_c}{\Theta_t^{7/3}} \qquad (13)$$

$$\text{with } B = \frac{0.216 \quad \alpha \; F \; n \; \delta\ell \; \delta\Omega}{A} \left(\frac{C}{kT_{Li}} \right)^{1/3}$$

in terms of the Li surface ionization efficiency, α.

Substituting $z = (\xi' - \gamma\xi_c)/\ell_2$ and $x = (\gamma h_c/\ell_2 z)^2$, Eq. (13) may be rearranged to read:

$$I_{Li}(\Theta) = \frac{B\ell_2^2}{\gamma^2} \int_{(\xi' - \gamma\xi_o)/\ell_2}^{(\xi' + \gamma\xi_o)/\ell_2} \frac{dz}{z^{4/3}}$$

$$\int_0^{(\gamma h_o/\ell_2 z)^2} \frac{dx}{x^{1/2}(1 + x)^{7/6}}. \qquad (14)$$

For relatively small values of Θ ($\Theta \lesssim 10°$), the upper limit on the intergration over x will always be greater than unity; under these circumstances, this upper limit may be replaced by infinity to a fairly good approximation, whereupon the integral over x becomes a Beta function and is easily evaluated. The integral over z is then straight-forward and Eq. (14) reduces to

$$I_{Li}(\Theta) = 7.77 \; \frac{B\ell_2^2}{\gamma^2} \quad F(\Theta, \Theta_R) \qquad (15)$$

where the form factor for small angle scattering is given in terms of the FWHM Li beam resolution angle, $\Theta_R = \xi_o/\ell_1 \simeq \gamma\xi_o/\ell_2$, by

$$F(\Theta, \Theta_R) = \frac{1}{(\Theta - \Theta_R)^{1/3}} - \frac{1}{(\Theta + \Theta_R)^{1/3}}. \qquad (16)$$

Then, comparisons of Eqs. (4), (7), and (15) indicate that the proper normalization factor is to be calculated by

$$\kappa = 0.42\ (\alpha/\beta)\ \frac{\ell_2^2}{(\ell_1 + \ell_2)^2}\ \ \frac{\ell_1}{h_o\ \Theta_R}\left(\frac{C}{kT_{Li}}\right)^{1/3}\ \frac{F(\Theta, \Theta_R)}{I_{Li}\ (\Theta)}. \qquad (17)$$

Figure 14 illustrates the good agreement between the experimental $I_{Li}\ (\Theta)$ curves and the small angle intensity form factor given in Eq. (16). The disagreement between intensities measured at positive and negative angles for very small values of Θ is probably caused by very small uncertainties in the determinations of the absolute positions of $\Theta = 0°$. The experimental curves begin to deviate from the theoretical expression in the vicinity of $\Theta \gtrsim 10°$, where some of the approximations employed in the development given above are expected to begin to fail. Figure 14 illustrates that normalization factors evaluated from Eq. (17) should be independent of the value of Θ chosen for comparison for $\Theta \lesssim 8°$. On the other hand, normalization constants evaluated on the basis of Eq. (9) would clearly be dependent on the particular value of Θ chosen[27].

Method B

As a second method of calculating reaction cross sections, we have used Method B of Ref. 10c. In this method, the normalization factor is obtained by comparisons of experimental and theoretical total cross sections,

$$\kappa = Q_{t,\,abs}^{eff} / Q_{t,\,rel}. \qquad (18)$$

The absolute effective total cross sections, $Q_{t,abs}^{eff}$, were calculated from expressions given in Ref. 10c for a van der Waals interaction. The total relative cross sections were obtained by integrating the sum of the Li and LiI signals over 4π steradians; after correcting for possible differences in ionization efficiencies, this becomes

$$Q_{t,rel} = 2\pi \int_0^{\pi} ((\beta/\alpha)\, I_{Li}(\theta) + I_{LiX}(\theta)) \sin\theta \, d\theta. \qquad (19)$$

Since scattering events were observed only if they deflected the Li or LiX out of the parent Li beam, the lower limit of integration in Eq. (19) was taken as $\theta_R = (m/\mu)\,\Theta_R$. In this aspect the current procedure differs slightly from Method B of Ref. 10c where a lower limit of $\theta = 1.61\,\theta_R$ was used for the integration.

Derived Values of Q_R

Table III gives values of the total reaction cross sections evaluated by the two methods (Q_R (A) from Eq. (17), Q_R (B) from Eq. (18)), using $\alpha/\beta = 1.0$ and $\theta_R = 1°$. The experimental geometry parameters used in Eq. (17) were (in cm.): 0.39, 4.5, and 39.3 for h_o, ℓ_1, and ℓ_2 respectively. The force constants C were calculated from the Slater-Kirkwood approximation (the reliability of this approximation is discussed in Ref. 10c) with the effective number of electrons taken as follows: 1 for Li; 14 for Cl_2, ICl, and Br_2; 26 for PCl_3; and 32 for $SnCl_4$. The polarizability values used were (in $\mathring{A}^3$): 20 for Li[28]; 4.6 for Cl_2[10a]; 7.5 for ICl[10d]; 6.2 for Br_2[10c]; 13.8 for $SnCl_4$[29]; and 11.5 for PCl_3[30]. The induction terms were calculated using dipole moments of 0.65 and 0.80 Debyes for ICl and PCl_3 respectively[31].

Table III indicates that reactive cross sections evaluated by Methods A and B are in close agreement, with the exception of Li + PCl_3 where the agreement is not as good. It is especially important in studies of Li atom reactions by crossed beams to obtain agreement between two independent methods of calculating reactive cross sections because this provides a check on the assumption of equal ionization efficiencies for Li and LiX. This assumption was invoked in interpreting previous studies of the other alkali metal reactions as well. With the possible exception of the Na study, this assumption was more plausible in previous studies because the alkali species were

much more efficiently ionized; consequently, their ionization efficiencies were expected to be much less sensitive to possible surface contaminants on the W and to the chemical identity and degree of internal excitation (which might be as much as 1 or 2 e.v.) of the alkali halides. Since the values of Q_R (A) and Q_R (B) listed in Table III were derived by assuming that α/β = 1.0, Eqs. (17) and (18) indicate that they are related to the true reactive cross section Q_R by

$$Q_R/Q_R(A) = \alpha/\beta = 1 + Q_{t,abs}^{eff} \frac{(Q_R(B) - Q_R(A))}{Q_R(B)\ Q_R(A)}. \qquad (20)$$

In the absence of any other errors in Q_R (A) and Q_R (B), Eq. 20 would yield values for (α/β) of 1.03, 0.88, 0.51, 0.75, and 2.67 for the LiX from Li + Cl_2, ICl, Br_2, $SnCl_4$, and PCl_3 respectively. In view of the other important possible sources of error in Q_R (A) and Q_R (B) and of the lack of any trend in these numbers, these results suggest that (α/β) was in fact close to unity.

In addition to questions of relative ionization efficiencies, there are a number of other important sources of error in the derived reactive cross sections. Errors of a different magnitude for each gas, but contributing the same percentage error to Q_R (A) and Q_R (B), may arise from uncertainties in the values of the van der Waal's force constants used. However, the derived values of Q_R depend primarily on the cube root of C; consequently, uncertainties in the values of the force constant contribute only a small error to the derived reactive cross

sections. Method A relies on a knowledge of the shape of the parent Li beam and in fact approximates the true beam shape by a beam of constant flux over a cross section of $4\,\xi_o\,h_o$ at the collision zone. Uncertainties in the "best" values of ξ_o and especially h_o may result in an uncertainty of as much as 25% in the values of Q_R (A) listed in Table III, although this effect should contribute the same percentage error for each of the five gases. Errors of the order of 10% are introduced into the values of Q_R (B) by uncertainties in the proper lower limit of integration in Eq. (19); another possible error of the order of 10% in the Q_R (B) values arises from the very large uncertainties in the shape of the L_{Li} (θ) curves for $\theta \gtrsim 30°$. The FVA transformation procedure, because it approximates the true E' distribution by a delta function distribution, introduces further errors; this effect is discussed in Ref. 24a. In general, this can represent a major source of error in derived reactive cross sections if the LAB↔CM transformation Jacobian varies appreciably in calculating the LAB distribution by integrating over the CM E' distribution. However, because of the nature of the transformation diagrams shown in Figs. 7-11 as well as the relatively high product velocities found for these Li reactions, this effect is only another minor source of uncertainty ($\sim$ 10-20%) in the Li Q_R values listed in Table III.

In summary, the absolute reaction cross sections derived here are uncertain, but are thought to be closer than a factor of two to the true values of Q_R; moreover, the ratio of derived Q_R values for any two gases should be somewhat more

accurate than are the individual values. In view of the similarities of $Q_{t,abs}$ and Q_R for Li + ICl and Br_2 shown in Table III, it is difficult to account for the differences in the undulatory behavior of the energy dependence of the Li + ICl and Br_2 total cross sections reported in Ref. 5 in terms of a quenching of this "glory structure" for Li + Br_2 due to more extensive chemical reaction.

DISCUSSION

Implications of the "Harpooning Model"

The very large cross sections for reaction between an alkali atom and halogen containing molecules which were initially observed in the Polanyi diffusion flame studies and later in crossed beam studies have been understood in terms of an electron transfer mechanism[1a]. In this picture, the attacking neutral reactants approach on a covalent potential curve which is crossed by an ionic curve at very large internuclear separation; at this point, the alkali atom transfers an electron to the halogenated molecule and the reaction becomes an ion recombination collision. Since the van der Waals interaction is very weak at large separations, this crossing radius is given approximately in terms of the ionization potential of the atom and the vertical electron affinity of the molecule by

$$e^2/r_c = I - E_v. \qquad (21)$$

In its crudest form, this model predicts a reactive cross section of πr_c^2.

Reactive cross sections for all five alkali atoms are plotted in Fig. 15 against the predictions of this model. The data does indicate a rough trend in Q_R with different alkali atoms which correlates with this electron transfer model. One disconcerting aspect of this model which was recognized[1a] at an early stage in the interpretation of the K, Rb, and Cs results was the relatively high vertical electron affinities necessary to fit the observed values of Q_R; in general, values of E_v were demanded which were a factor of two or so higher than those suggested by other estimates. This effect becomes especially troublesome for the Li data reported here; as Fig. 15 indicates, these reactive cross sections imply extremely high estimates of E_v, between 70 and 80 kcal/mole for $SnCl_4$, ICl, and Br_2.

These large values of Q_R might be understood in terms of an electron jump model with more moderate estimates of the vertical electron affinities if one takes into account the variation of the neutral potential curve with internuclear distance. An approximate maximum impact parameter which leads to reaction is given by $(Q_R/\pi)^{1/2}$; in order to invoke the participation of the ionic curve, the trajectory on the neutral potential curve for this impact parameter and the incident collision energy must penetrate to an internuclear separation as small as the curve crossing radius, r_c. Neglecting the effect of the repulsive core of the neutral collision potential, the long range attractive van der Waal's force eliminates all

restrictions on r_c for Li + PCl_3 for collision energies above 0.6 kcal/mole, since the neutral partners would approach all the way to r = 0 for all impact parameters less than $(Q_R/\pi)^{1/2}$. However, it represents only a minor correction for the other four reactions studied; the required values of r_c are lowered by ~ 10% for Li + Cl_2 and by ~ 5% for the other three gases. The solution to this dilemma is probably best understood in terms of a perturbation of the neutral potential curve by the ionic curve at distances greater than the crossing radius of the two curves. Provided that this perturbation provides enough additional attraction to overcome the centrifugal repulsion associated with the large reactive impact parameters found in these studies, the reactants could be attracted to within the crossing radius. Studies[32] of elastic scattering of K from some reactive molecules have provided some experimental evidence of a lowering of the long-range neutral potential curve due to a perturbation by the ionic curve.

Possible Mass Effects

The data listed in Table I, although only rough indications of the energy partitioning, do indicate that the Li reactions studied here channel most of the available reaction exothermicity into product excitation; furthermore, for a fixed reactant gas, these results indicate monotonically increasing product recoil energy as the mass of the attacking atom decreases. Both the magnitude of the final recoil energies found in LiX products and the trends in the energy partitioning as the alkali mass

is varied conflict with the predictions of the spectator stripping mechanism[11,1a] and the elastic spectator model[33] which were used to account, at least in part, for the energy partitionings observed in early crossed beam studies of the K, Rb, and Cs + X_2 reactions. Monte Carlo calculations suggest that the data in Table I may be understood in terms of a greater fraction of the product repulsive energy release appearing as recoil energy as the mass of the attacking atom decreases.

Early Monte Carlo calculations, employing potential surfaces which were not chosen to refer to the alkali atom-halogen molecule reactions, indicated a mass dependent energy partitioning in qualitative accord with the data of Table I. Blais and Bunker[34] reported an "energy anomaly" which led to a much larger fraction of the total energy released appearing as product recoil whenever the mass of the attacking atom was considerably smaller than that of either atom in the reacting molecule. Kuntz, et. al.[35] reported a detailed Monte Carlo study of the energy partitioning in an exchange reation. In very qualitative terms, they observed that energy liberated during reactant approach was channelled into product vibration, whereas energy liberated during product separation was divided between internal excitation and product recoil energy; the fraction of this "repulsive energy release" appearing as product recoil increased as the mass of the attacking atom was decreased.

Direct investigations of the mass dependence of the energy partitioning in alkali atom-halogen molecule reactions by Monte Carlo calculations are not available as yet. Blais[36] did

report calculations for K, Rb, and Cs + Br_2 and I_2 and observed no appreciable mass effect; Godfrey and Karplus's calculations[37] are restricted to K + Br_2. Polanyi and co-workers have not yet reported in detail on their calculations for these reactions. However, they have observed[38] that "second encounters" between the MX and Y products of the reaction M + XY are a relatively common feature of the trajectories of these reactions for their potential energy surface and that these secondary encounters often produce appreciably higher recoil energies; it seems plausible that due to the faster approach of Li^+ to the dissociating XY^- and to the faster oscillations of LiX, Li reactions might be especially susceptible to this effect.

The magnitudes of the reactive cross sections and the attenuations of the wide-angle elastic scattering indicate that qualitatively similar very strong, long-range attractive forces are operative as the reactants approach for all of the alkali atoms. In view of this, it is plausible to attribute the very much broadened LiX CM angular distributions to a mass effect in the overall reaction dynamics. This might arise as the Li atom, by virtue of its light mass, is rapidly accelerated during reaction and may well reach the other reactant before it has had an opportunity to dissociate. In this context, we have examined an ultra simple model of these reactions based on a linear M - XY collision with harmonic oscillator forces between MX and XY. For fixed forces (80% of the reaction exothermicity as M - X attraction, 20% as X-Y repulsion) and fixed X and Y masses a normal coordinates analysis of the motion indicates

that both the fraction of the reaction exothermicity which appears as product recoil energy and the lifetime of the collision increase as the mass of the attacking atom is decreased from Cs to Li. The former feature of this model correlates qualitatively with the trends in Table I. The increasing collision lifetime suggest a broadened angular distribution and so agrees with the experimental results shown in Figs. 12 and 13.

However, with respect to the three diatomic halogen reactions, alternate possible interpretations of the broadened LiX distributions are suggested by the recent Monte Carlo studies. Godfrey and Karplus[37] report that their calculations indicate a rough correlation of increasing angle of deflection of the product with decreasing impact parameter in the collision. Since the Li atom reactions are evidently restricted to smaller impact parameters than are the corresponding K, Rb, or Cs reactions, this could account for the depletion of the MX small angle scattering in the case of Li reactions. Indeed, this interpretation is supported by the observation that, if the curves in Fig. 12 are replotted as absolute differential cross sections, it is observed that the wide angle LiX scattering is always less than that of the corresponding K, Rb, or Cs halide product at the same angle. A second possible objection to the assignment of a broadened LiX product distribution to a mass factor is provided by the Monte Carlo calculation on $K + I_2$ reported by Blais[36] which indicates that the KI product distribution broadens as the dipole-induced dipole attraction between the products is weakened. Since the ratios of dipole moments for LiCl to KCl and

LiBr to KBr are about 0.7 and 0.6 respectively, this effect could explain the broadened product distributions in the Li + Cl_2, Br_2 and ICl reactions. It would appear essential that Monte Carlo studies be extended to Li "stripping reactions" in order to determine the relative importance of mass effects, distributions of impact parameters, and small changes in the product forces in the resultant shape of the product angular distributions. Experimentally, detailed comparisons of Li and Na reactive scattering as well as the concurrent depletion of elastic scattering should help to elucidate the origins of the broadened product distributions reported here.

The Li + $SnCl_4$ and PCl_3 product distributions no longer peak at 0° and their overall shapes are indicative of more complex collision trajectories. The LiCl LAB distribution from Li + PCl_3 may be adequately fit by a CM distribution symmetric about θ = 90°; this is of course the distribution which would be produced if the reaction proceeded through formation of a complex which were long-lived with respect to a rotational period. A number of reactions[39] of neutral species are now known to proceed via this complex mechanism, although these reactions have given product angular distributions which peaked at θ = 0° and 180°; this has been interpreted in terms of the break-up of a polate symmetric top complex, whose angular momentum projection onto the symmetry axis of the molecule was partitioned according to a thermal equilibrium in the critical instant immediately prior to break-up. The present study appears to provide the first example[40] of a symmetric CM

product distribution which peaks at $\theta = 90°$. Within the framework of this collision complex model, this is the predicted[39] angular distribution for the breakup of an oblate symmetric top complex. Oblate tops occur much less frequently in chemistry than do prolate tops; however, reasonable assumed structures for a PCl_3Li complex (maintaining the PCl_3 C_{3v} symmetry) do have an oblate top structure, whereas replacement of the Li atom by a heavier alkali atom would render them prolate tops. Thus, the symmetric CM distribution fit to the LAB distribution observed here, if corraborated by more detailed experiments, might indicate the first reaction to proceed via an oblate top complex mechanism.

However, this simple picture is clouded somewhat by the $Li + SnCl_4$ results presented here. While these results cannot be fit adequately at wide LAB angles by a symmetric LiCl CM distribution, the LiCl distributions from $Li + SnCl_4$ and PCl_3 are similar, suggesting that both reactions may proceed via a similar mechanism. The $Li + SnCl_4$ results might be understood in terms of an osculating complex model, where the complex lifetime is comparable to a rotational period. The Cs + TlX reactions have been discussed[41] in terms of the breakup of an osculating prolate complex; although this model has not been discussed for the breakup of an oblate top, it could probably account for the $Li + SnCl_4$ data of Fig. 13. However, in contrast to the $Li + PCl_3$ case, it is difficult to account for a $LiSnCl_4$ complex which is oblate rather than prolate; an oblate structure appears to require a rather substantial distortion of the

geometry of $SnCl_4$ upon complex formation (e.g., relaxation to a planar -$SnCl_3$ structure).

In summary, the Li reactions studied here exhibit the same broad qualitative features shown by the Na, K, Rb, and Cs reactions. However, interesting differences are indicated in the energy partitionings and the product angular distributions. Future experiments employing electric deflection and velocity selection analysis will make possible measurements of the distribution functions for product translational and rotational energies as well as more definite angular distribution measurements and should resolve some of the questions raised by the present study.

ACKNOWLEDGEMENTS

We are indebted to Mr. Shen-Maw Lin, L. C-H Loh, and C.A. Mims for help in the collection and analysis of some of the data presented here and for many informative discussions. This work was supported by the Atomic Energy Commission.

REFERENCES

1. See, for example, the following reviews: (a) D.R. Herschbach, Adv. Chem. Phys. 10, 319 (1966); (b) E.F. Greene and J. Ross, Science 159, 587 (1968); (c) J.P. Toennies, Ber. Bunsenges. Physik. Chem. 72, 927 (1968).
2. M. Polanyi, Atomic Reactions (Williams and Norgate, London, 1932); C.E.H. Bawn, Ann. Rept. Chem. Soc. (London) 39, 36 (1942).
3. J.H. Birely, E.A. Entemann, R.R. Herm, and K.R. Wilson, J. Chem. Phys. (to be published).
4. For a recent review, see: R.B. Bernstein, Adv. Chem. Phys. 12, 389 (1967).
5. R.K.B. Helbing and E.W. Rothe, J. Chem. Phys. 48, 3945 (1968).
6. An early attempt to study Li + CH_3I in crossed beams was unsuccessful; K.R. Wilson (unpublished work), Lawrence Radiation Laboratory, Berkeley, California, 1962.
7. Preliminary results of this work have been reported in: D.D. Parrish and R.R. Herm, J. Chem. Phys. 49, 5544 (1968).
8. K. Ljalikov and A. Terenin, Z. Physik 40, 107 (1926).
9. Some information on gas phase Li chemistry is available from seeded flame studies; see, for example, D.E. Jensen and P.J. Padley, Trans. Far. Soc. 62, 2132 (1966).
10. (a) For K, Rb, and Cs + Cl_2: R. Grice and P.B. Empedocles, J. Chem. Phys. 48, 5352 (1968); (b) for K, Rb, Cs + ICl: G.H. Kwei, Ph.D. thesis, University of California, Berkeley, 1967; G.H. Kwei and D.R. Herschbach, J. Chem. Phys. (to be

published); (c) for K, Rb, Cs + Br_2: J.H. Birely, R.R. Herm, K.R. Wilson, and D.R. Herschbach, J. Chem. Phys. 47, 993 (1967); (d) for Na + ICl, Br_2: Ref. 3; (e) for Cs + $SnCl_4$ and Rb + PCl_3: K.R. Wilson and D.R. Herschbach, J. Chem. Phys. 49, 2676 (1968).

11. R.E. Minturn, S. Datz, and R.L. Becker, J. Chem. Phys. 44, 1149 (1966).

12. R.J. Gordon, R.R. Herm, and D.R.Herschbach, J. Chem. Phys. 49, 2684 (1968).

13. A standard 1" Swadgelok fitting was used to couple the liquid nitrogen fill tube to the reservoir; this provided a leak-tight seal even after repeated thermal cycling.

14. K.R. Wilson and R.J. Ivanetich, UCRL Rept. 11606, University of California Radiation Laboratory, Berkeley, 1964.

15. S.G. Andresen and C.A. Shipley, Rev. Sci. Instr. 36, 858 (1965).

16. This magnet was almost identical to that described in: M.A.D. Fluendy, R.M. Martin, E.E. Muschlitz, Jr., and D.R. Herschbach, J. Chem. Phys. 46, 2172 (1967).

17. Even in the absence of this pressure broadening effect, the transmission would be expected to vary slightly with Θ because the laboratory energy of elastically scattered Li varies with Θ; this effect is analyzed in Ref. 12.

18. This mass spectrometer is patterned after that described by: C.F. Giese and W.B. Maier, II, J. Chem. Phys. 39, 739 (1963).

19. The ions were detected on a resistance strip electron

multiplier purchased from the Bendix Corporation, Cincinnati Ohio; this multiplier showed no deterioriation after repeated low pressure exposures to the alkali metal and halogen vapors employed in these experiments.

20. It should be pointed out that these error bars are not intended to indicate the total uncertainty in the data. Other errors may contribute as well, although uncertainties in T_H (Θ) probably comprise the primary source of errors.

21. This may not be quite valid since, at the source pressures used, the velocity distribution may be somewhat distorted due to a "Laval" effect (see Ref. 12 for an example). Possible modifications of the centroid distributions by this effect were not considered, however, because the centroid distributions are included only for qualitative comparisons with the product angular distributions.

22. S. Datz, D.R. Herschbach, and E.H. Taylor, J. Chem. Phys. 35, 1549 (1961).

23. As a cautionary note, it should be pointed out that any appreciable amount of inelastic scattering of the high velocity Li atoms in the vicinity of $\Theta = 0$ could give anonomously low values for the derived reactive scattering.

24. (a) E.A. Entemann, Ph.D. Thesis, Harvard University, 1967; (b) E.A. Entemann and D.R. Herschbach, Disc. Far. Soc. 44, 289 (1967).

25. M.C. Moulton and D.R. Herschbach, J. Chem. Phys. 44, 3010 (1966).

26. Part of the treatment given here is similar to that given in R. Helbing and H. Pauly, Z. Physik 179, 16 (1964).

27. No criticism of the procedure followed in Ref. 10 is intended as these workers employed much sharper alkali atom beams and thus were able to directly compare their small angle elastic scattering with the expected $\Theta^{-7/3}$ dependence.

28. B. Bederson and E.J. Robinson, Adv. Chem. Phys. 10, 1 (1966).

29. Landolt - Börnstein Zaklenwerte und Functionen, A.M. Hellwege and K.H. Hellwege, Eds. (Springer - Verlag, Berlin), Vol. 1, Part 3 (1951), p. 510 ff.

30. Calculated from dielelectric constants of pure liquid PCl_3 reported by T.M. Lowry and J. Hofton, J. Chem. Soc., 207 (1932).

31. C.H. Townes and A.L. Schawlow, Microwave Spectroscopy (McGraw-Hill, New York, 1955).

32. E.F. Greene, L.F. Hoffman, M.W. Lee, J. Ross, and C.E. Young (to be published).

33. D.R. Herschbach, Appl. Optics, Suppl. 2 (Chemical Lasers), 128 (1965).

34. N.C. Blais and D.L. Bunker, J. Chem. Phys. 39, 315 (1963).

35. P.J. Kuntz, E.M. Nemeth, J.C. Polanyi, S.D. Rosner, and C.E.Young, J. Chem. Phys. 44, 1168 (1966).

36. N.C. Blais, J. Chem. Phys. 49, 9 (1968).

37. M. Godfrey and M. Karplus, J. Chem. Phys. 49, 3602 (1968).

38. P.J. Kuntz, M.H. Mok, E.M. Nemeth, and J.C. Polanyi, Disc. Far. Soc. 44, 229 (1967).

39. W.B. Miller, S.A. Safron, and D.R. Herschbach, Disc. Far. Soc. 44, 108 (1967).

40. With the possible exception of the K + CCl_4 reaction; see Ref. 10e.

41. G.A. Fisk, J.D. McDonald, and D.R. Herschbach, Disc. Far. Soc. 44, 228 (1967).

TABLE I. Estimates of Recoil Energies[a]

Reaction	Li Atoms			E'			
	E	ΔD_o	E'	Na	K	Rb	Cs
$M + Cl_2 \rightarrow MCl + Cl$	1.94	54	7.6		3.6	2.1	1.7
$M + ICl \rightarrow MCl + I$	2.00	61	2.2	1.5	1.7	2.0	1.5
$M + ICl \rightarrow MI + Cl$	2.00	34	24.	13.5	13.6	12.8	8.4
$M + Br_2 \rightarrow MBr + Br$	2.00	54	6.6	5.1	3.7	2.8	1.8
$M + SnCl_4 \rightarrow MCl + SnCl_3$	2.03	35	2.3				
$M + PCl_3 \rightarrow MCl + PCl_2$	1.99	33	5.2				

[a]All energies are given in kcal/mole. E is the initial relative kinetic energy of the reactants corresponding to the most probable source velocities. E' is the product recoil energies estimated from the FVA transformation procedure; all data for Na, K, Rb, and Cs were taken from Ref. 10. $\Delta D_o = D_o(MX) - D_o(RX)$ is the reaction exothermicity. Bond dissociation data were taken from: for LiX, L. Brewer and E. Brackett, Chem. Rev. 61, 425 (1961); for halogen molecules, G. Herzberg, Spectra of Diatomic Molecules (D. van Nostrand Co., Inc., Princeton, N.J., 1950); for the polyhalides, T.L. Cottrell, The Strengths of Chemical Bonds (Butterworth Scientific Publications, London, 1958).

TABLE II. LiX CM Distribution Expansion in Legendre Polynomials[a]

Reactant	a_o	a_1	a_2	a_3	a_4	a_5
Cl_2	0.625	0.470	-0.035	0.004	-0.060	-0.004
ICl	0.634	0.351	0.011	0.041	-0.031	-0.006
Br_2	0.706	0.482	-0.038	-0.053	-0.072	-0.025
$SnCl_4$	1.037	0.422	-0.435	0.104	0.013	-0.142
PCl_3	1.239	0.209	-0.469	0.138	-0.084	-0.035

[a]These coefficients are defined by $I_{LiX}(\theta) = \Sigma_n a_n P_n(\cos\theta)$ and are normalized such that $\Sigma_n a_n = 1$.

TABLE III. Total and Reactive Scattering Cross Sections[a]

System	$\langle E^{-1/3} \rangle^{-3}$	C	$Q_{t,\,abs}$	$Q_{t,\,abs}^{eff}$	$Q_R(A)$	$Q_R(B)$
$Li + Cl_2$	2.57	460	454	244	86	87
Li + ICl	2.73	730	546	284	130	123
$Li + Br_2$	2.71	610	496	266	146	115
$Li + SnCl_4$	2.73	1350	700	341	165	147
$Li + PCl_3$	2.71	1140	656	331	43	55

[a]The mean elastic collision energies, $\langle E^{-1/3} \rangle^{-3} = 1.36\ (\mu/m)\ kT_{Li}$, are given in kcal/mole, the van der Waals force constants in 10^{-12} ergs/Å^6 and the cross sections in Å^2. The total cross section was calculated for the relative velocity corresponding to $\langle E^{-1/3} \rangle^{-3}$.

FIGURE CAPTIONS

Fig. 1. Diagram of the apparatus, as viewed from above. The reactant beams, which cross at an angle $\gamma = 90°$, effuse from ovens mounted on a platform which may be rotated from $\Theta = -55°$ to $\Theta = +120°$ with respect to the stationary deflecting magnet and detector assembly. Only scattering in the plane of the reactant beams is measured and the sense of Θ depicted in this figure is taken as positive, with $\Theta = 0°$ in the direction of the Li atom beam. The entire detector assembly (ionizing filament, ion optics, analyzing magnet, electron multiplier, and electrical shield) may be scanned across the gap of the deflecting magnet in order to measure beam profiles and deflection patterns.

Fig. 2. Plot of the viewing factor (ratio of total collision volume to that seen by the detector) against Θ. The circles give calculated values of $V(\Theta)$ based upon the Li beam profile predicted by slit geometry and two gas beam profiles: (1) the profile calculated from slit geometries (open circles) and (2) a typical measured profile (13° FWHM; dark circles). The squares are experimental values of $V(\Theta)$ determined by averaging $V(\Theta)$ values measured during about twenty-five separate studies of the scattering of Li from various gases; the error bars give the standard deviations in these average values. The circles are normalized to the squares to give the best overall fit.

Fig. 3. Comparison of the angular distribution of NaBr from Na + Br_2 measured in this work by magnetic deflection analysis (open circles) normalized to the more conventional two-filament differential surface ionization results reported in Ref. 3 (dark circles).

Fig. 4. Primary data for Li + Br_2, corrected for the viewing factor. The x's show the total intensity at zero magnetic field. Also shown are data for the transmitted intensity at high field (◊, ▽, ●) for three separate experiments and the derived non-reactive Li signal (□, ▲, ○ connected by the solid curve).

Fig. 5. Primary data for Li + Cl_2, ICl, $SnCl_4$, and PCl_3, corrected for the viewing factor. The x's show the total intensity (Li + LiX); the symbols show the derived Li intensity (the solid curves represent the "average" Li angular distribution). For Li + Cl_2 and ICl, the circles and triangles report data from independent experiments.

Fig. 6. Plot of CM angular distributions (plotted as $I_{Li}(\theta)$ sin θ) for the elastic scattering, derived by transforming the solid smooth curve fit to the LAB data for Li atom scattering shown in Figs. 4 and 5; data taken from the LAB curves at 5° intervals was transformed. The open circles were obtained from LAB data with $\Theta > 0°$, the dark circles from data with $\Theta < 0°$. The data was linearly extrapolated to $\theta = 180°$ (dashed lines). The Li + cyclohexane curve was obtained by transforming LAB data not given in Fig. 4 or 5 and was normalized to agree with the Li + Cl_2 angular distribution at narrow angles.

Fig. 7. LAB angular distribution of LiCl product from Li + Cl_2, derived from data presented in Fig. 5; the solid curve through the data points indicate the "best" distribution, based on analysis of the error in each data point. The error bars indicate the uncertainty introduced by errors in the measurement of the transmission of Li atoms through the field, $T_H(\Theta)$. The dotted curve gives the calculated distribution in centroid angles for an energy independent collision cross section. The dashed curve is back-calculated from the derived CM distribution shown in Fig. 12. Also plotted is a kinematic diagram showing the most probable reactant source velocities, the corresponding centroid vector $\underset{\sim}{C}$, and the relative velocity vector $\underset{\sim}{V}$; the circles indicates the length of the LiCl recoil velocity for a few of the possible product recoil energies E' (kcal/mole). The two Li temperatures refer respectively to runs without and with the deflecting magnet.

Fig. 8. Calculated centroid distribution and LAB angular distribution of LiX product from Li + ICl, derived from data of Fig. 5. The solid curve through the data points gives the "best" distribution; the dashed curve is back-calculated from the CM distribution shown in Fig. 12. Error bars indicate uncertainties introduced by errors in the determination of $T_H(\Theta)$. Also shown is a kinematic diagram of some of the possible LiX recoil velocities: solid circles for LiCl product; dashed circles for LiI product.

Fig. 9. Calculated centroid distribution, kinematic diagram, and LAB angular distribution of LiBr from Li + Br_2, derived

from data of Fig. 4. Solid curves indicate "best fits" to the data; the dip near $\Theta = 0°$ is thought to be real, but both solid curves were transformed into the CM distributions shown in Fig. 12. The dashed and the dotted curves give the corresponding back-calculated LAB distributions. The error bars reflect uncertainties in the determination of $T_H(\Theta)$.

Fig. 10. Calculated centroid distribution, kinematic diagram, and LAB angular distributions of LiCl from Li + $SnCl_4$, derived from data of Fig. 5. The solid curve gives the "best" experimental distribution; the dashed curve was back-calculated from the derived CM distribution shown in Fig. 13. Error bars reflect uncertainties in measurements of $T_H(\Theta)$.

Fig. 11. Calculated centroid distribution, kinematic diagram, and LAB angular distribution of LiCl from Li + PCl_3, derived from data of Fig. 5. Error bars reflect uncertainties in measurements of $T_H(\Theta)$. The solid line gives the "best" experimental distribution; the dashed curve below the solid curve at large values of Θ was back-calculated from the derived CM angular distribution shown in Fig. 13. The dashed curve somewhat higher than the solid curve at large values of Θ is back-calculated for the same E' (5.2 kcal/mole) from the CM angular distribution symmetric about $\Theta = 90°$ in Fig. 13; this dashed curve joins the other dashed curve to the left of the peak in the centroid distribution.

Fig. 12. Comparison of CM product angular distributions: the Li data were obtained by transforming the solid curves of

Figs. 7, 8, and 9 at 5° intervals by the FVA procedure; the heavier alkali data were taken from Ref. 10. The open circles refer to positive CM angles (rotations of the recoil velocity vector counter-clockwise from the original Li direction); the dark circles refer to negative values of θ. The data was extrapolated to $\theta = 180°$ from the last open circle data point.

Fig. 13. Comparisons of CM product angular distributions: Li data from Figs. 10 and 11; Rb + PCl_3 and Cs + $SnCl_4$ data from Ref. 10; transformation procedure the same as for Fig. 12. The dashed symmetric curve for Li + PCl_3 was back-calculated as well (see Fig. 11) to test for a possible "long-lived complex" mechanism for this reaction.

Fig. 14. Comparison of the narrow angle elastic scattering relative intensity form factor, $F(\Theta,\Theta_R)$ of Eq. (16), with experimental $I_{Li}(\Theta)$ curves (normalized to $F(\Theta,\Theta_R)$) for four of the scattering partners studied. Open symbols are for $\Theta > 0°$; closed symbols for $\Theta < 0°$. A $\Theta^{-7/3}$ dependence has been normalized to F (5°, 1°) for comparison. For Li + Cl_2 and $SnCl_4$ (not shown in the Fig.), the agreement is equally good.

Fig. 15. Families of curves showing the variation of reactive cross section, as predicted by the elementary form of the electron transfer mechanism, Eq. (21), with ionization potential for different assumed values of the vertical electron affinity. For Li, $Q_R(A)$ data from Table III are plotted. For the other alkali atoms, $Q_R(A)$ data of Ref. 10 are shown as open symbols; for Cs + Cl_2, where the agreement between Methods A and B was especially bad, the $Q_R(B)$ value is plotted as well as the dark triangle.

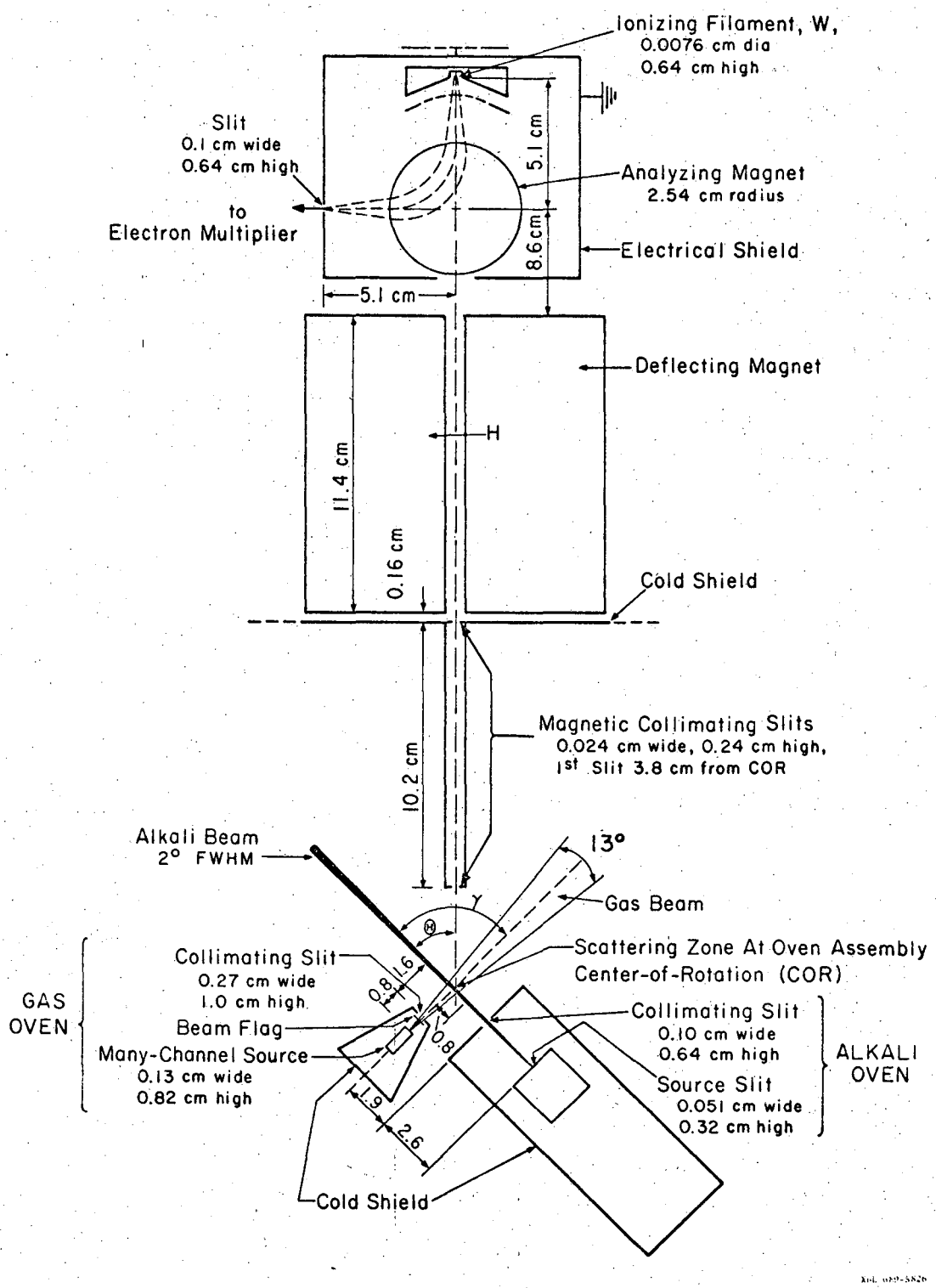
Ionizing Filament, W,
0.0076 cm dia
0.64 cm high
Slit
0.1 cm wide
0.64 cm high
to
Electron Multiplier
5.1 cm
Analyzing Magnet
2.54 cm radius
8.6 cm
Electrical Shield
5.1 cm
Deflecting Magnet
H
11.4 cm
0.16 cm
Cold Shield
Magnetic Collimating Slits
0.024 cm wide, 0.24 cm high,
1st Slit 3.8 cm from COR
10.2 cm
Alkali Beam
2° FWHM
13°
Gas Beam
Collimating Slit
0.27 cm wide
1.0 cm high
Scattering Zone At Oven Assembly
Center-of-Rotation (COR)
GAS
OVEN
Beam Flag
Many-Channel Source
0.13 cm wide
0.82 cm high
Collimating Slit
0.10 cm wide
0.64 cm high
Source Slit
0.051 cm wide
0.32 cm high
ALKALI
OVEN
Cold Shield

Fig. 1

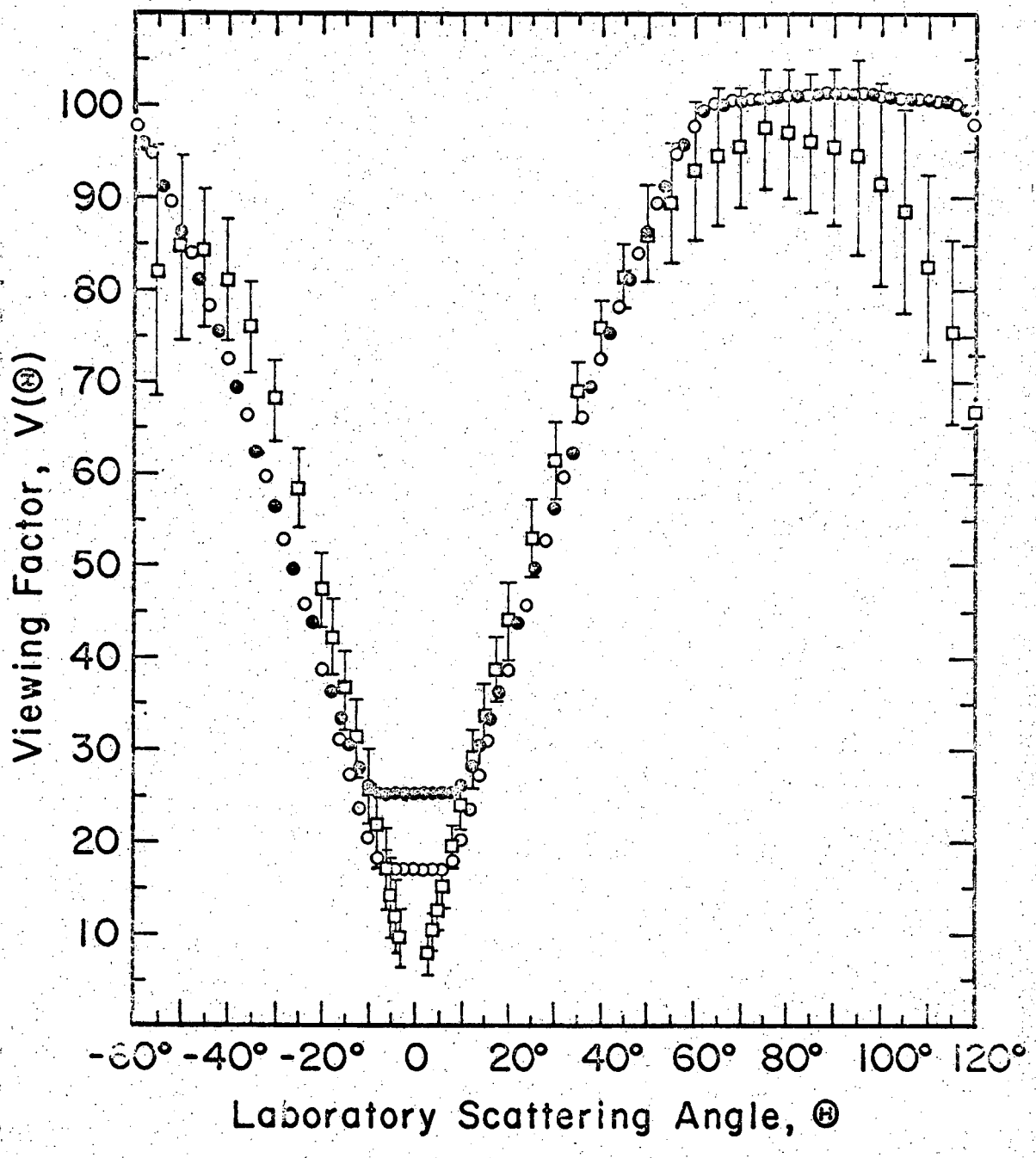

XBL 689-1827

Fig. 2

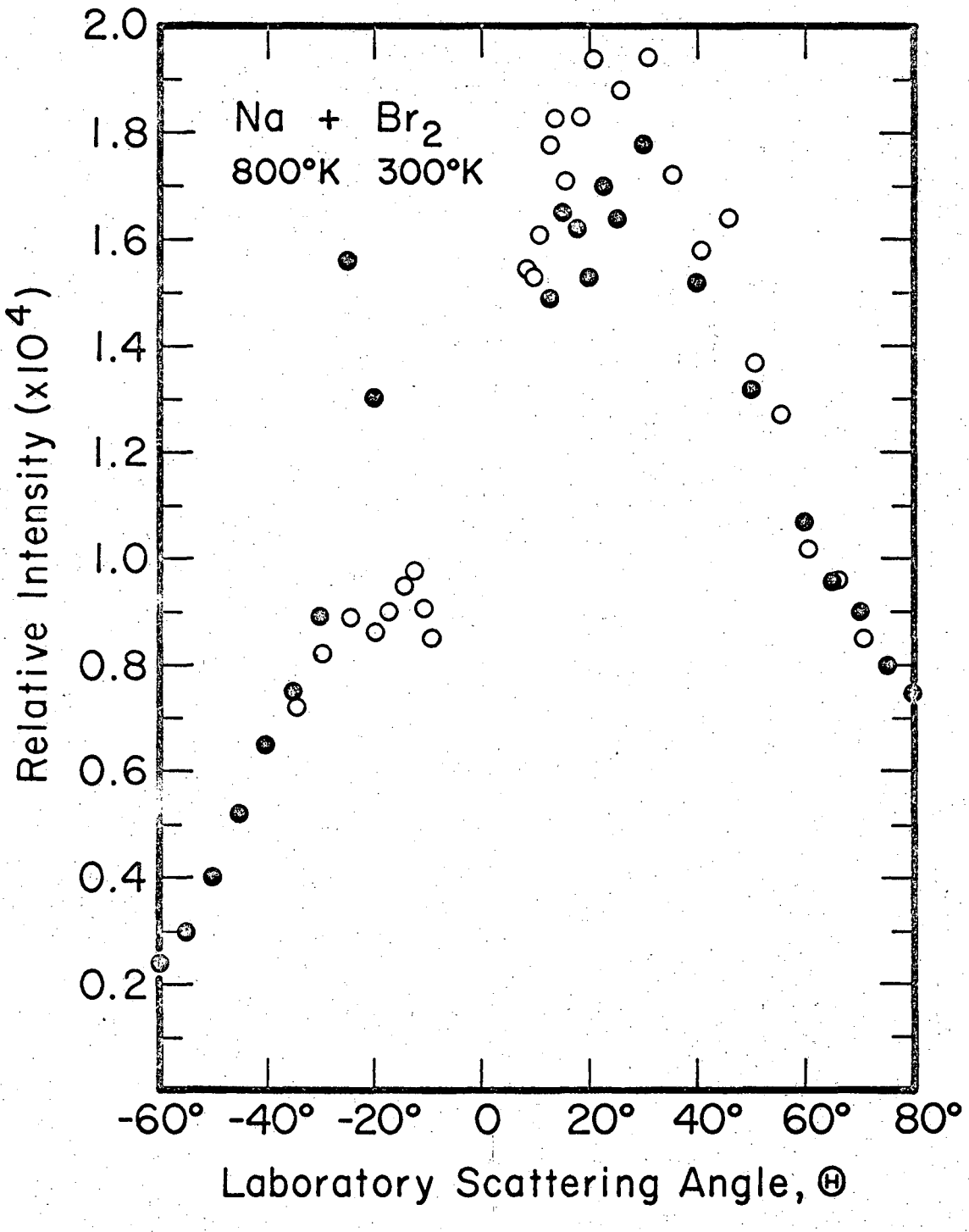

XBL 689-5828

Fig. 3

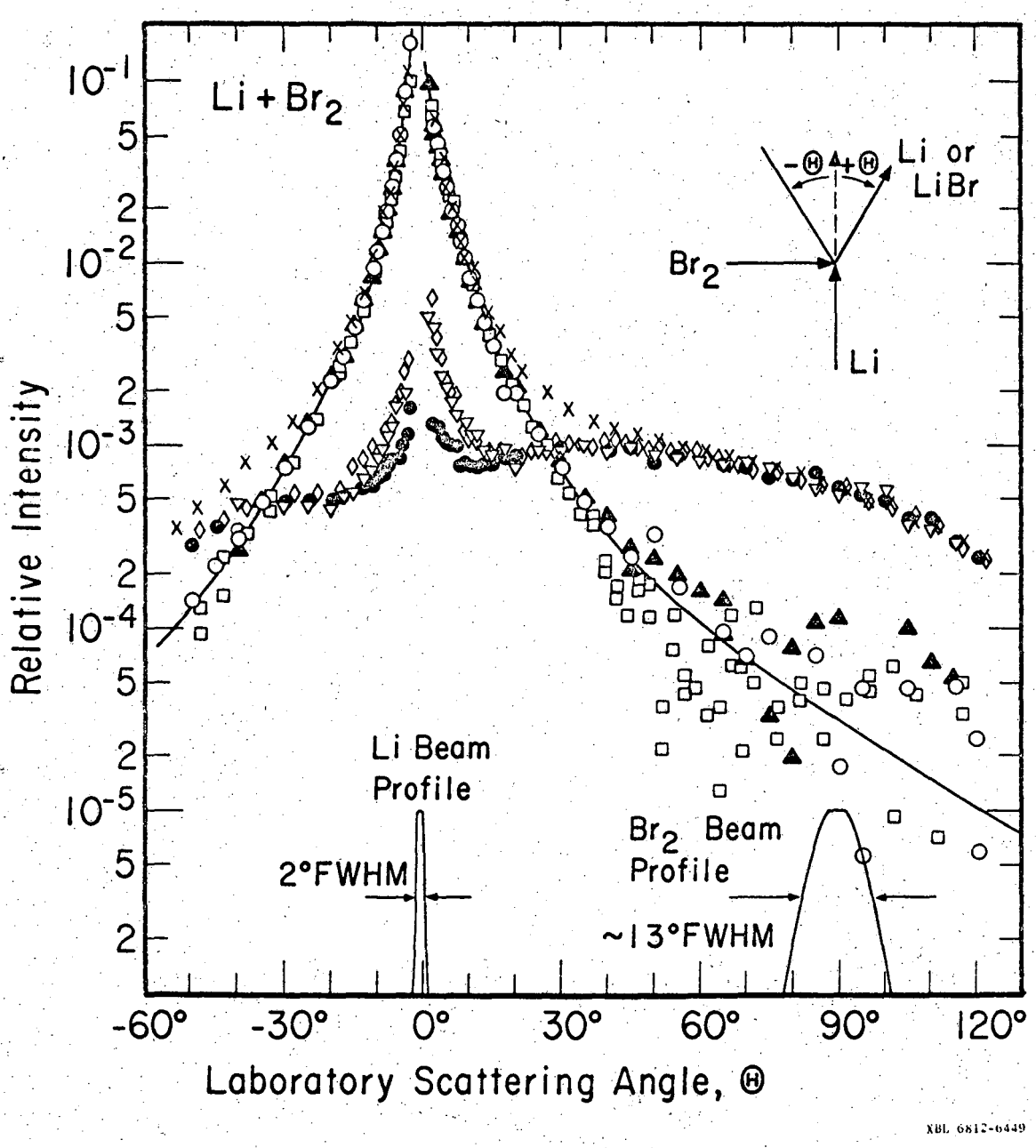
Li + Br2
Relative Intensity
10-1
5
2
10-2
5
2
10-3
5
2
10-4
5
2
10-5
5
2
Li or LiBr
Br2
Li
Li Beam Profile
2°FWHM
Br2 Beam Profile
~13°FWHM
-60°
-30°
0°
30°
60°
90°
120°
Laboratory Scattering Angle, Θ
XBL 6812-6449

Fig. 4

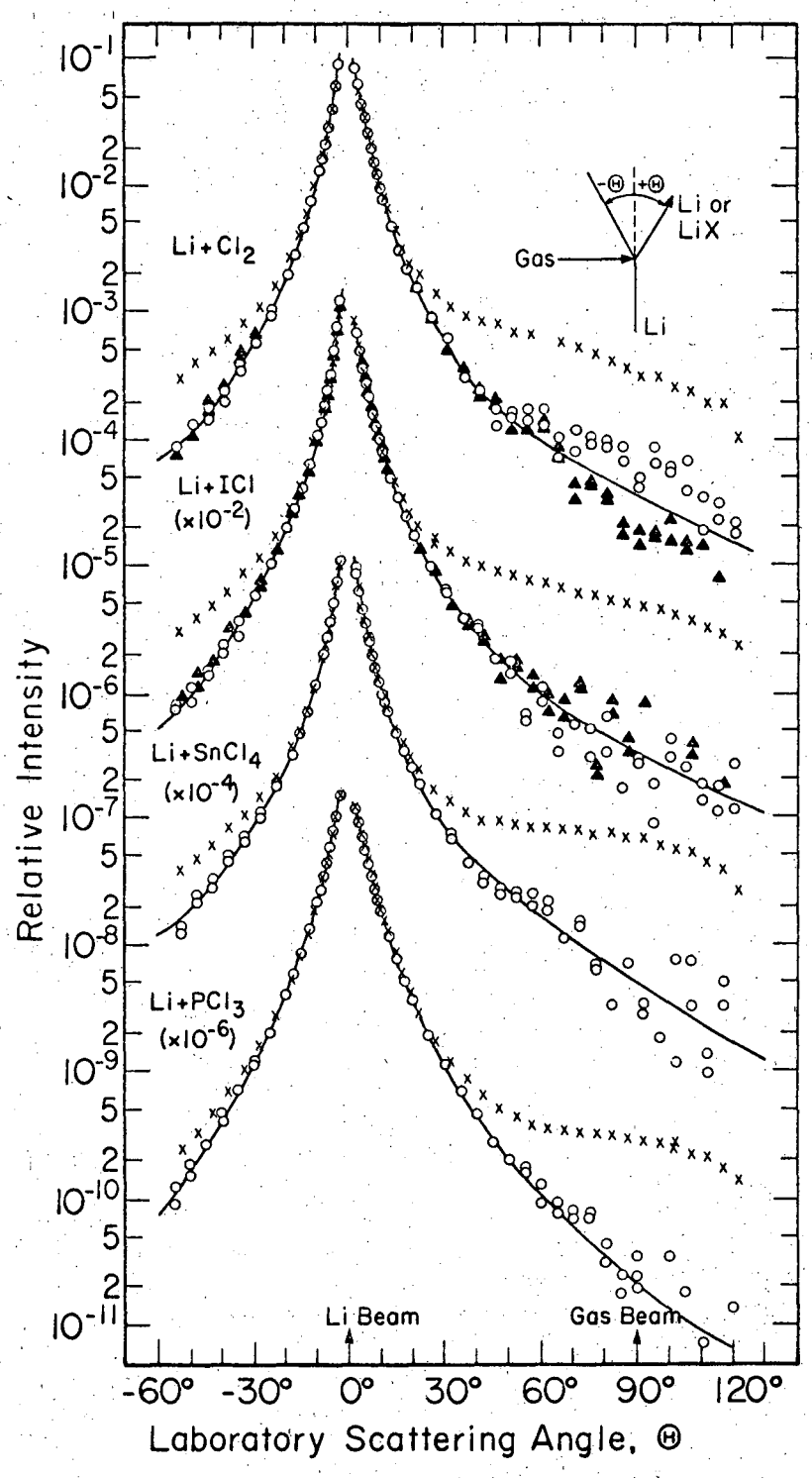

XBL 6812-6451

Fig. 5

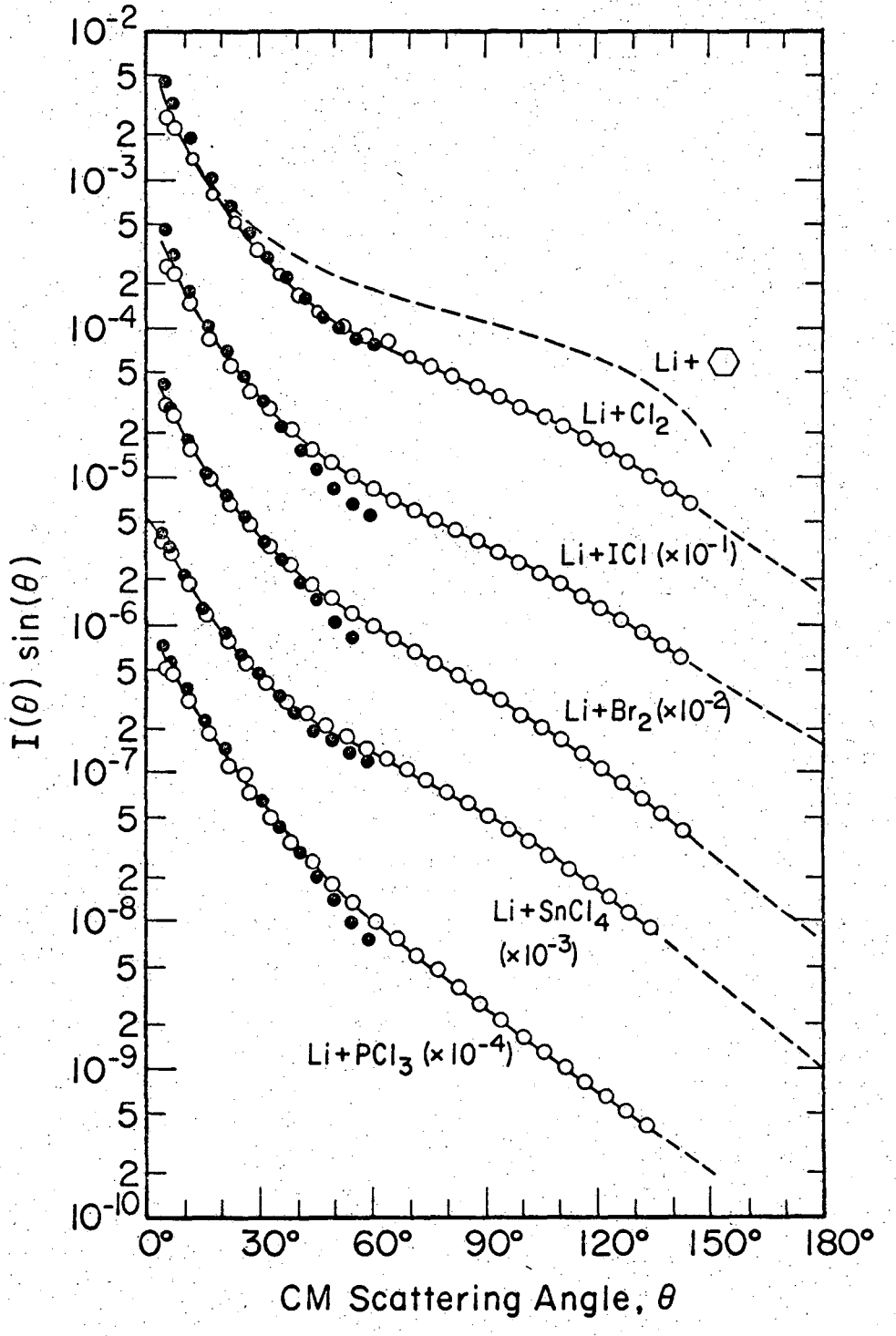

XBL 6812-6450

Fig. 6

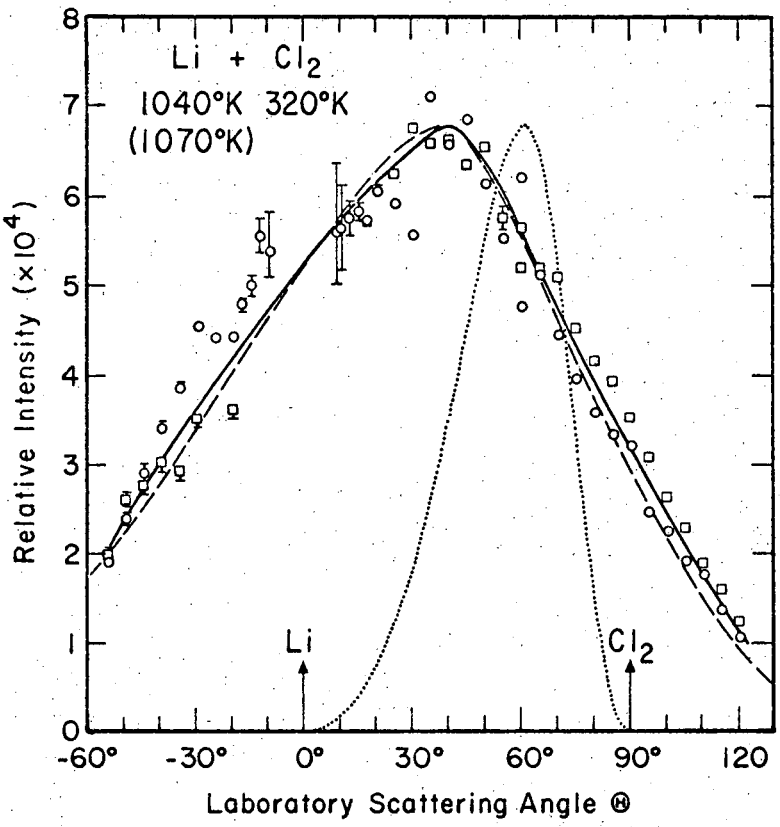

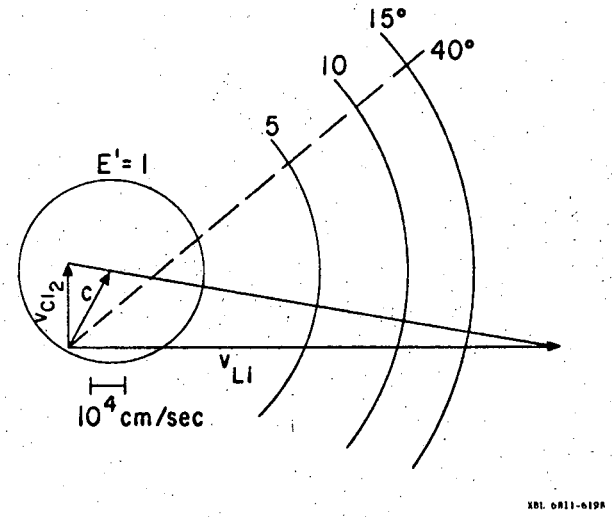

XBL 6811-6198

Fig. 7

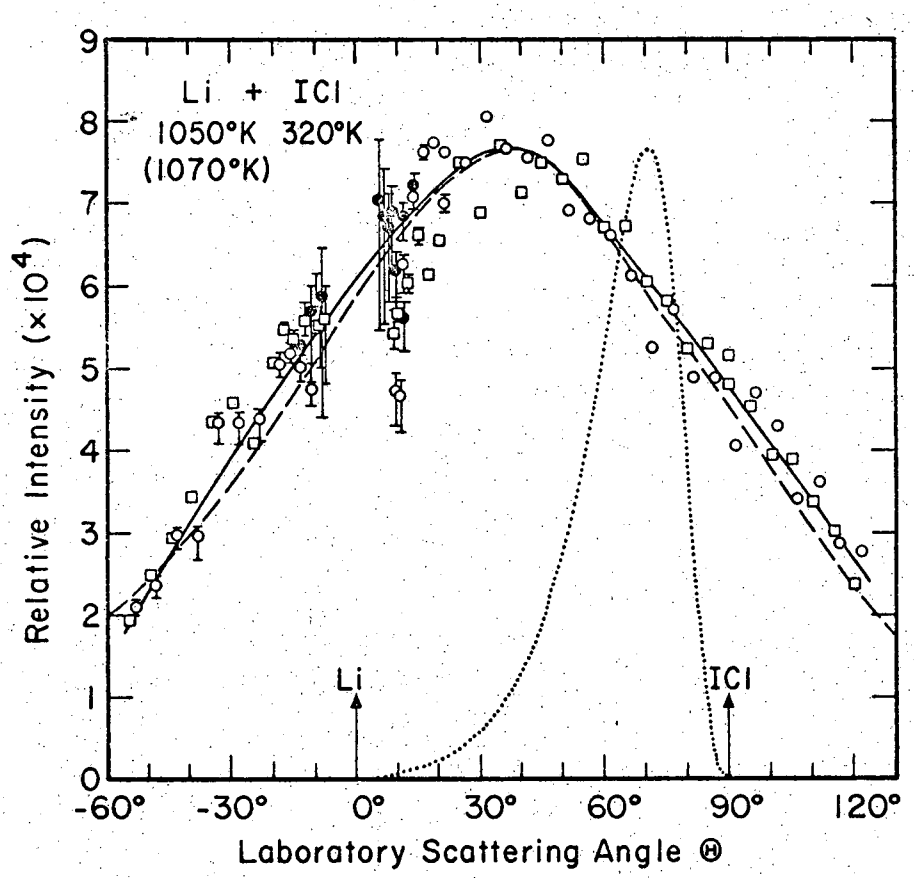

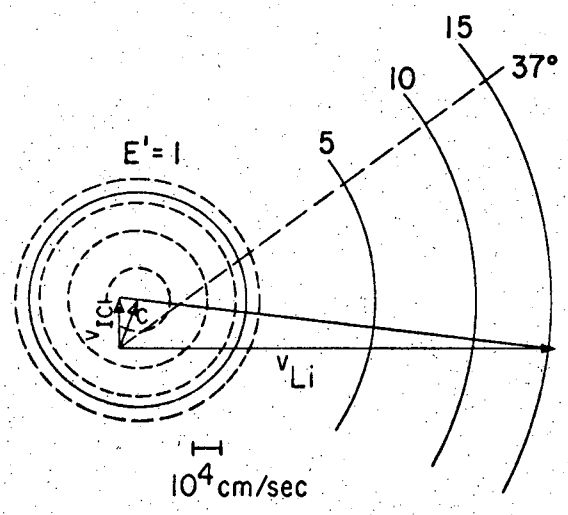

XBL 6811-6197

Fig. 8

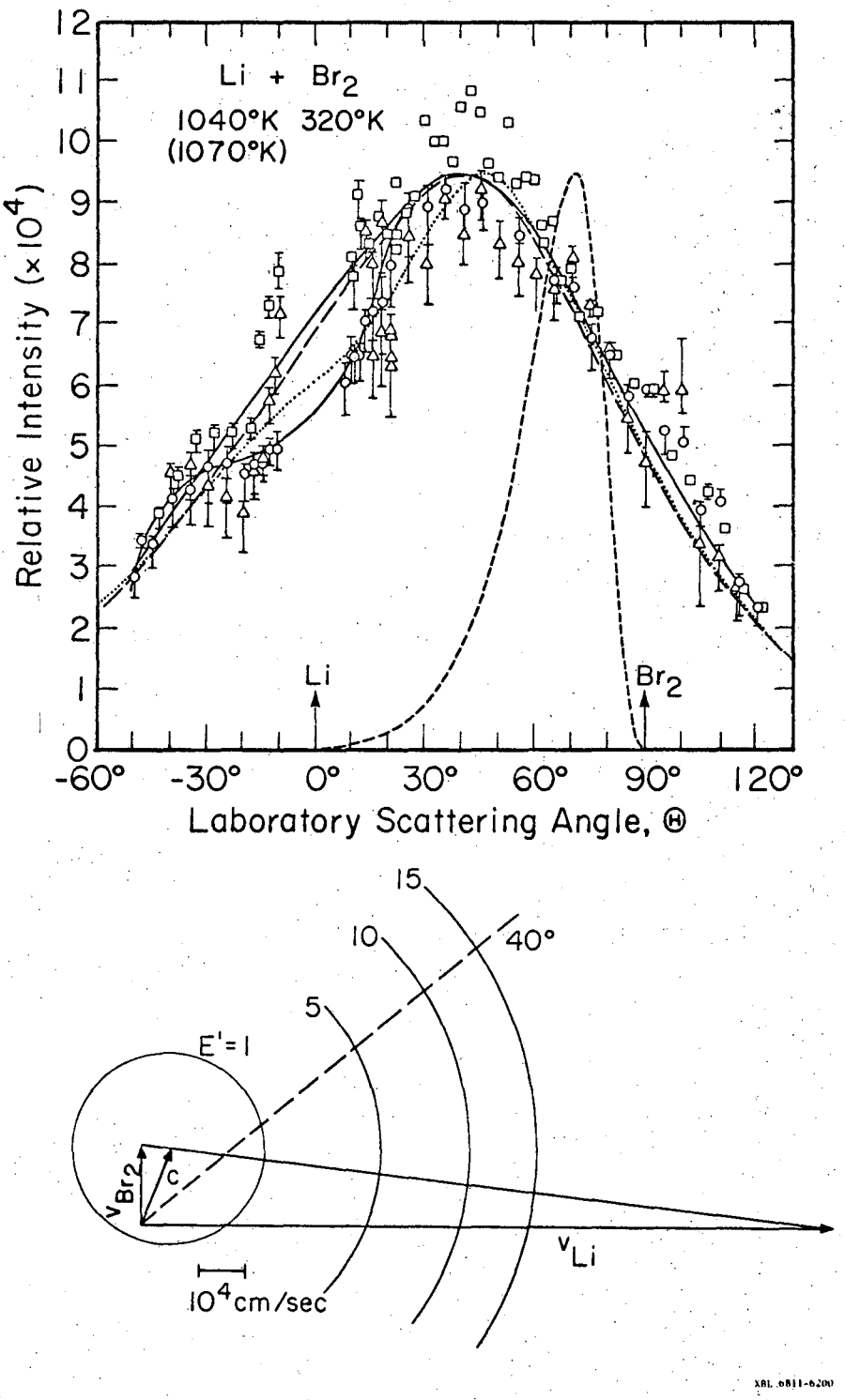
Li + Br2
1040°K 320°K
(1070°K)
Relative Intensity (×10^4)
Laboratory Scattering Angle, Θ
Li
Br2
-60°
-30°
0°
30°
60°
90°
120°
15
10
5
40°
E'=1
v_Br2
c
v_Li
10^4 cm/sec
XBL 6811-6200

Fig. 9

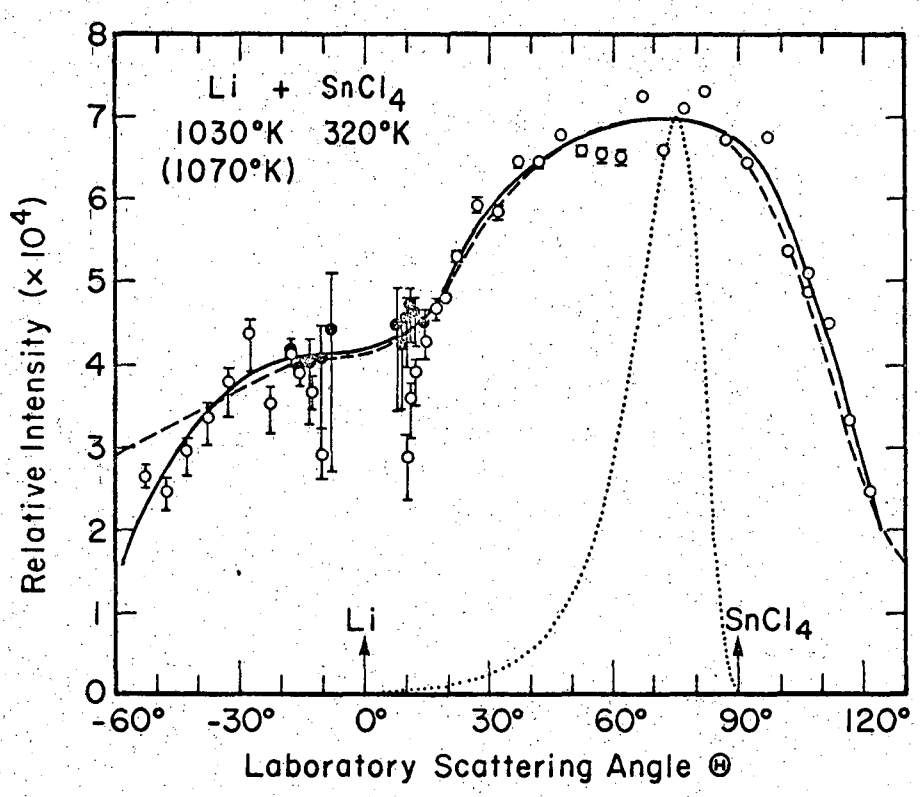

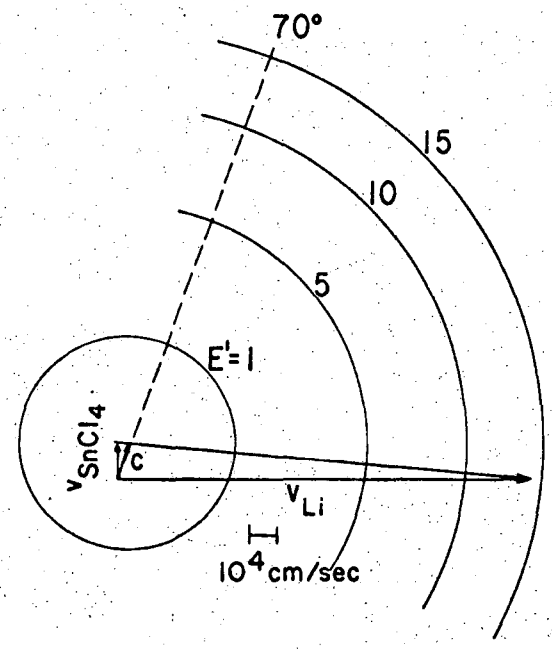

X6L 6811-6199

Fig. 10

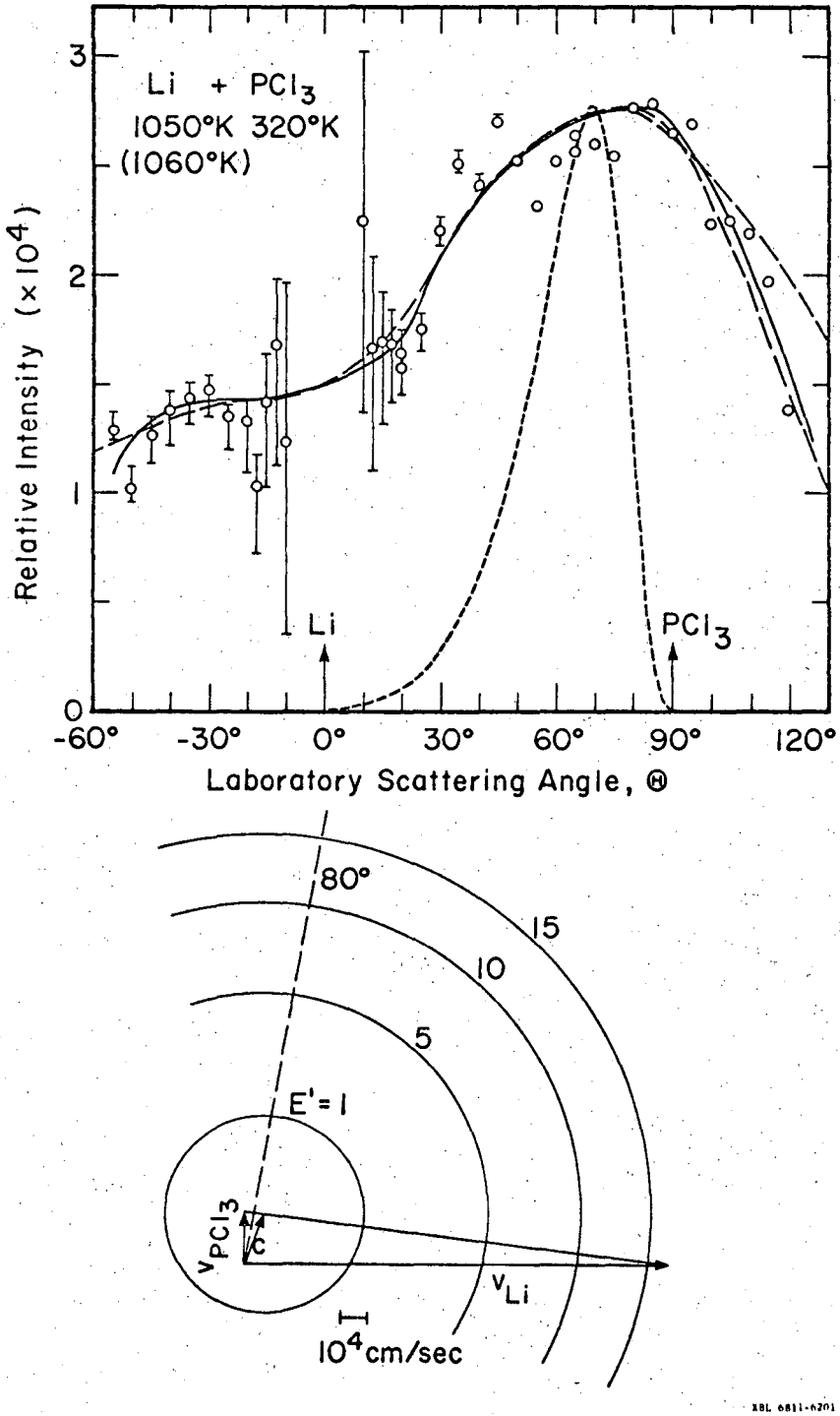
Li + PCl3
1050°K 320°K
(1060°K)
Relative Intensity (x10^4)
Li
PCl3
Laboratory Scattering Angle, Θ
80°
15
10
5
E'=1
v PCl3
c
v Li
10^4 cm/sec
XBL 6811-6201

Fig. 11

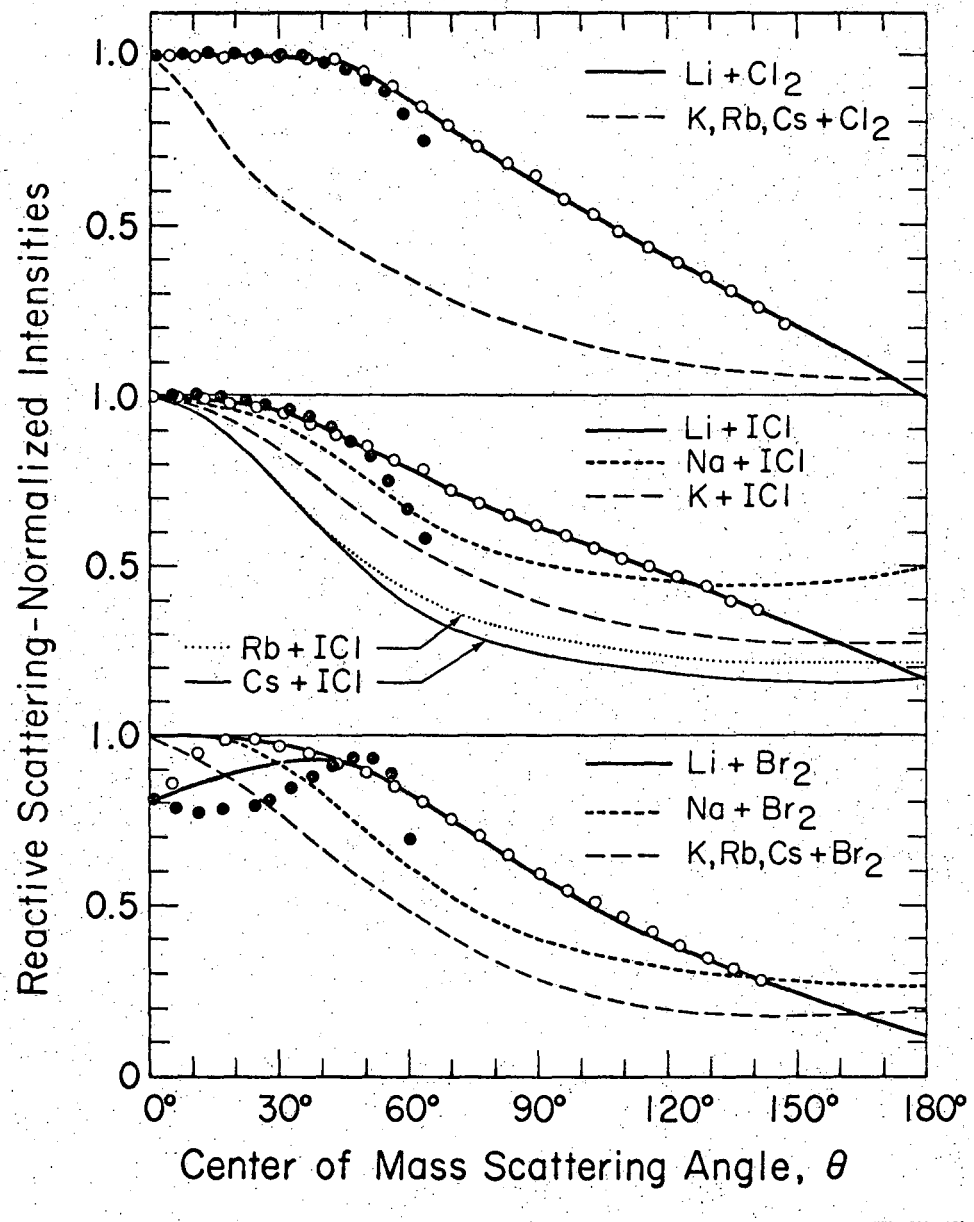
Reactive Scattering-Normalized Intensities
1.0
0.5
1.0
0.5
1.0
0.5
0
Li + Cl2
K, Rb, Cs + Cl2
Li + ICl
Na + ICl
K + ICl
Rb + ICl
Cs + ICl
Li + Br2
Na + Br2
K, Rb, Cs + Br2
0°
30°
60°
90°
120°
150°
180°
Center of Mass Scattering Angle, θ
XBL 6811-6135

Fig. 12

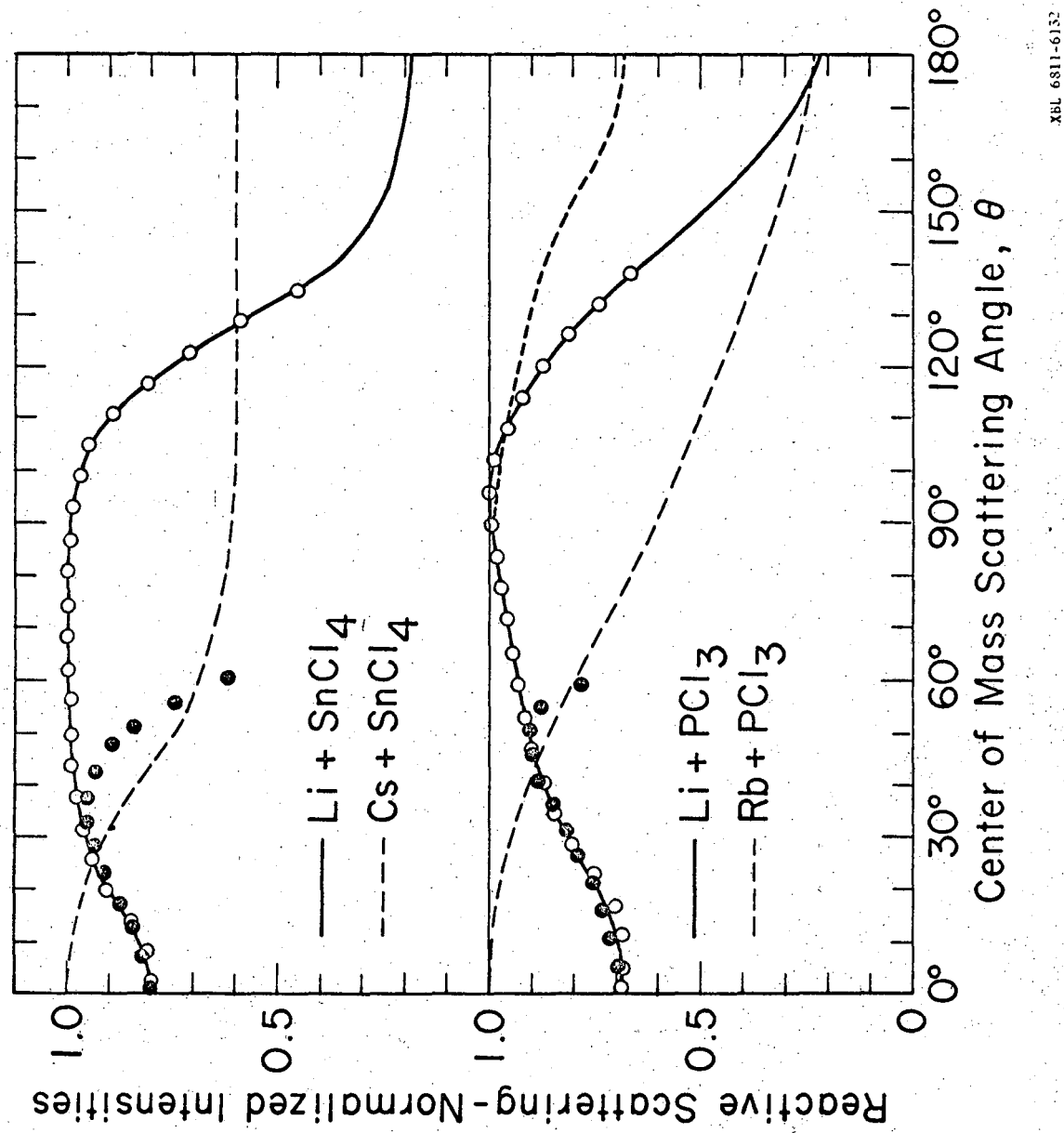
Reactive Scattering-Normalized Intensities
1.0
0.5
1.0
0.5
0
0°
30°
60°
90°
120°
150°
180°
Center of Mass Scattering Angle, θ
Li + SnCl4
Cs + SnCl4
Li + PCl3
Rb + PCl3
XBL 6811-6132

Fig. 13

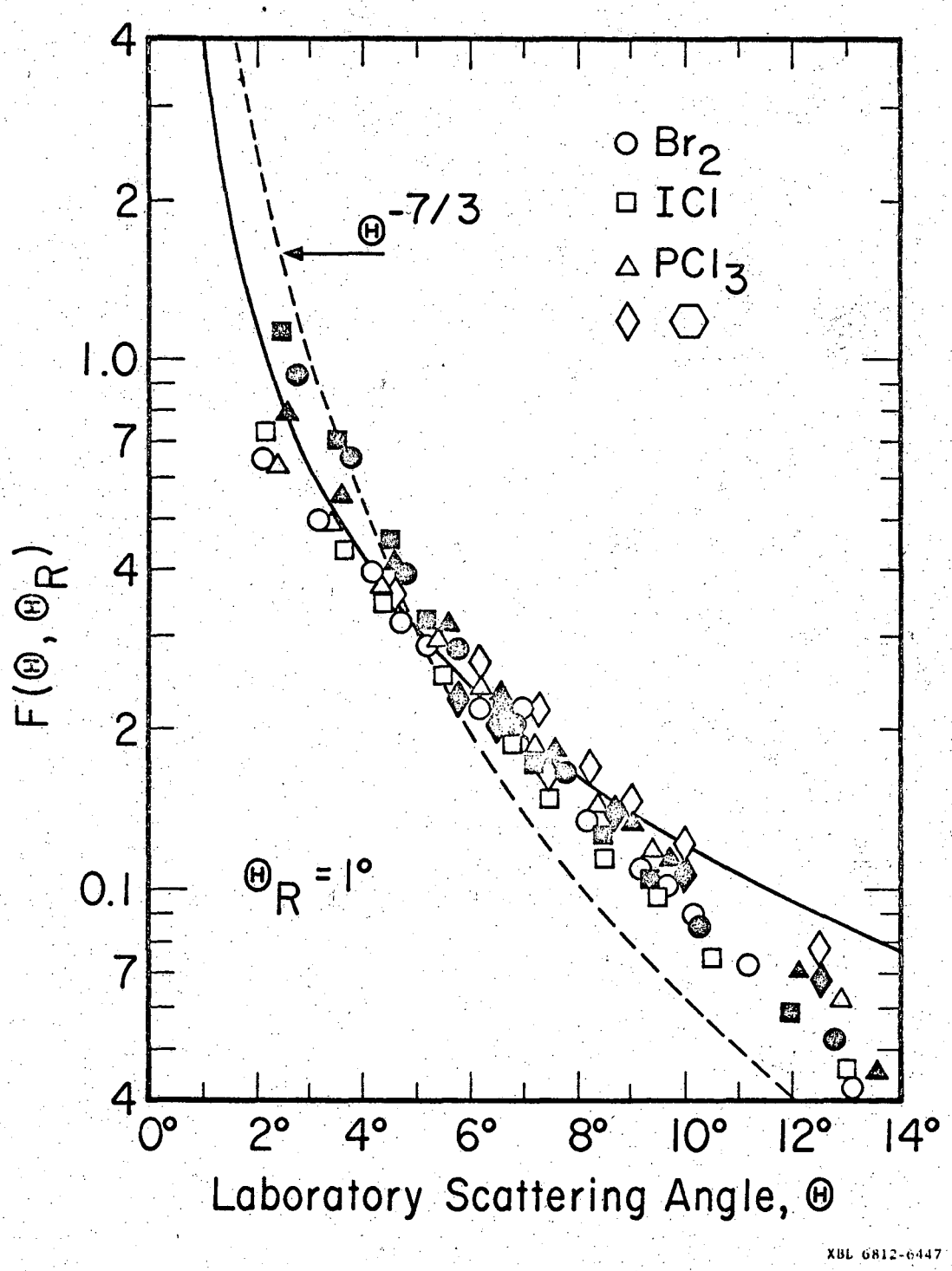
4
2
1.0
7
4
2
0.1
7
4
F(Θ, Θ_R)
Θ^-7/3
Br2
ICl
PCl3
Θ_R = 1°
0°
2°
4°
6°
8°
10°
12°
14°
Laboratory Scattering Angle, Θ
XBL 6812-6447

Fig. 14

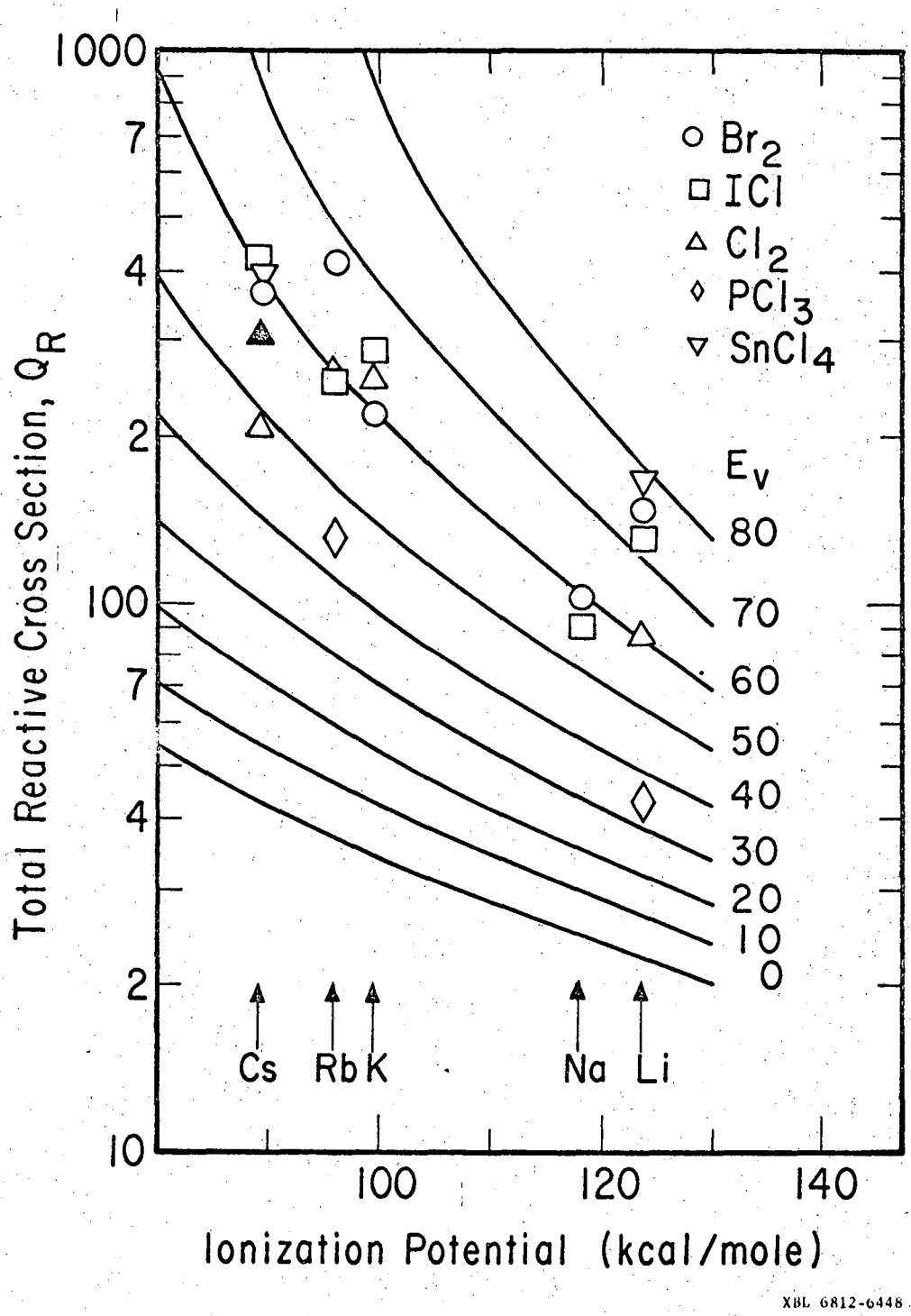
1000
7
4
2
100
7
4
2
10
Total Reactive Cross Section, Q_R
Br_2
ICl
Cl_2
PCl_3
$SnCl_4$
E_v
80
70
60
50
40
30
20
10
0
Cs
Rb
K
Na
Li
100
120
140
Ionization Potential (kcal/mole)
XBL 6812-6448

Fig. 15